AGU PUBLICATIONS

Tectonics

RESEARCH ARTICLE
10.1002/2016TC004264

Key Points:
- Structural data record a wrench-dominated transpressional zone in central Idaho
- Emplacement of syntectonic magmas facilitated partitioning of strain in the transpressional zone
- Zircon U-Pb data indicate main phase deformation at ca. 95–92 Ma and late-stage deformation at ca. 84 Ma

Supporting Information:
- Table S1
- Table S2

Correspondence to:
C. Ma,
macmachong@gmail.com

Citation:
Ma, C., D. A. Foster, P. A. Mueller, and B. L. Dutrow (2017), Magma-facilitated transpressional strain partitioning within the Sawtooth metamorphic complex, Idaho: A zone accommodating Cretaceous orogen-parallel translation in the Idaho batholith, *Tectonics*, *36*, 444–465, doi:10.1002/2016TC004264.

Received 7 JUN 2016
Accepted 20 FEB 2017
Accepted article online 23 FEB 2017
Published online 14 MAR 2017

©2017. American Geophysical Union. All Rights Reserved.

Magma-facilitated transpressional strain partitioning within the Sawtooth metamorphic complex, Idaho: A zone accommodating Cretaceous orogen-parallel translation in the Idaho batholith

Chong Ma[1,2], David A. Foster[1], Paul A. Mueller[1], and Barbara L. Dutrow[3]

[1]Department of Geological Sciences, University of Florida, Gainesville, Florida, USA, [2]Now at Department of Geosciences, Auburn University, Auburn, Alabama, USA, [3]Department of Geology and Geophysics, Louisiana State University, Baton Rouge, Louisiana, USA

Abstract Structural data from metasedimentary rocks and geochronologic data from intrusive rocks in the Idaho batholith provide evidence for the relationship between deformation and magmatism in the northern U.S. Cordillera. The Sawtooth metamorphic complex (SMC), Idaho, is exposed as an inlier in the central Idaho batholith and contains strongly deformed metasedimentary and intrusive rocks. Geologic mapping reveals north-south-striking, alternating contraction- and shear-dominated domains across strike. The contraction-dominated domains consist of centimeter- to tens of meter-scale, shallowly to steeply plunging upright folds with subhorizontal lineations. The shear-dominated domains are characterized by highly strained subvertical foliations, subhorizontal lineations, and syntectonic intrusive sheets. Pervasive S-C structures, winged porphyroclasts, and asymmetric folds indicate dextral strike-slip shearing. The fabrics in the two types of domains are structurally compatible and are interpreted to be broadly synchronous. This work suggests that the SMC structures represent a wrench-dominated transpressional zone, in which the regional strain partitioned into the contraction- and shear-dominated domains and the partitioning was facilitated by emplacement of syntectonic magmas. Zircon U-Pb data of the syntectonic intrusions indicate that the SMC transpressional deformation occurred mainly between ca. 95–92 Ma and ca. 84 Ma and had ended by ca. 77 Ma. The transpressional deformation in the SMC and the western Idaho shear zone (WISZ) were kinematically compatible and partially coeval. This suggests that the SMC and WISZ represent a regional transpression system and that crustal deformation inboard of the continental margin may have contributed to the northward orogen-parallel translation of accreted terranes during the Late Cretaceous.

1. Introduction

There is significant evidence that the oceanic and continental terranes accreted to the Cordilleran margin of North America in Mesozoic time were translated substantial distances to the north in Cretaceous time [e.g., *Oldow et al.,* 1989; *Saleeby and Busby-Spera*, 1992; *McClelland et al.,* 2000; *Dickinson*, 2004, 2006; *Gray and Oldow*, 2005; *Wyld et al.,* 2006]. In the northern U.S. Cordillera, the western Idaho shear zone (WISZ) played an important role in accommodating the Late Cretaceous dextral strike-slip displacement [*McClelland et al.,* 2000; *Giorgis et al.,* 2008] after Early Cretaceous accretion of arcs including the Blue Mountains composite terrane [e.g., *Lund and Snee*, 1988; *Manduca et al.,* 1993; *Getty et al.,* 1993]. The WISZ is characterized by north-south-striking, subvertical foliations with subvertical lineations after removal of the tilt caused by Miocene extension [*Tikoff et al.,* 2001]. The subvertical lineations suggest a strong margin-normal contractional component that reflects pure shear. Evidence for a margin-parallel wrench component corresponding to simple shear, however, seems to be less strong on the basis of that (1) strike-slip lineation is absent in the WISZ, (2) the strike-slip kinematic indicators are rare [*Lund and Snee*, 1988; *Giorgis et al.,* 2008], and (3) the available kinematic indicators are only developed locally on the edge of the WISZ [e.g., *McClelland et al.,* 2000]. Numerical modeling combined with field data suggests that the transpressional deformation of the WISZ had an angle of oblique convergence up to 60° [*Giorgis and Tikoff*, 2004; *Giorgis et al.,* 2016], indicating a large convergent component of deformation [*Fossen and Tikoff*, 1993; *Dewey et al.,* 1998]. *Giorgis and Tikoff* [2004] conclude that the WISZ might have experienced only about 50 km of margin-parallel strike-slip displacement. Overall, the contraction component was predominant over the wrench component in the WISZ [*Manduca et al.,* 1993; *McClelland et al.,* 2000; *Giorgis et al.,* 2008]. The exposed portion of WISZ therefore is

19449194, 2017, 3, Downloaded from https://agupubs.onlinelibrary.wiley.com/doi/10.1002/2016TC004264 by Auburn University Libraries, Wiley Online Library on [27/10/2022]. See the Terms and Conditions (https://onlinelibrary.wiley.com/terms-and-conditions) on Wiley Online Library for rules of use; OA articles are governed by the applicable Creative Commons License

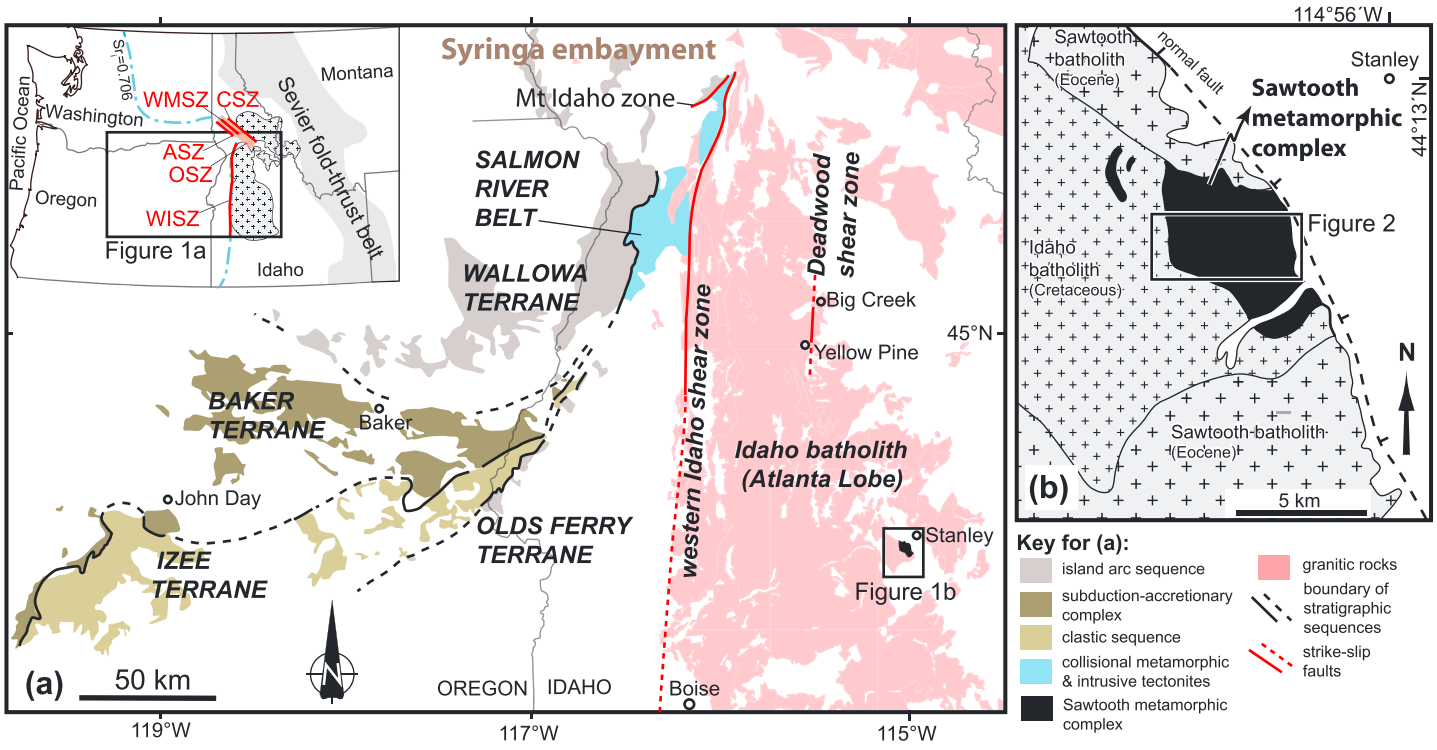

Figure 1. (a) Simplified geologic map of the Idaho batholith region and the Blue Mountains province. (b) Distribution of the Sawtooth metamorphic complex. Sources are *Fisher et al.* [1992]; *Lund et al.* [1997]; *LaMaskin et al.* [2011]; *Schmidt et al.* [2016], and "Digital Geology of Idaho" (http://geology.isu.edu/Digital_Geology_Idaho/). ASZ = Ahsahka shear zone, CSZ = Clearwater shear zone, OSZ = Orofino shear zone, WISZ = western Idaho shear zone, WMSZ = Woodrat Mountain shear zone.

a contraction-dominated rather than wrench-dominated transpressional shear zone [*Tikoff and Teyssier*, 1994; *Dewey et al.,* 1998; *Giorgis et al.,* 2005].

A limited amount of dextral movement recorded in the WISZ [*Giorgis et al.,* 2005] cannot solely accommodate several hundred kilometers of northward translation of accreted terranes that has been suggested by paleomagnetic and detrital zircon data [e.g., *Housen and Dorsey*, 2005; *LaMaskin et al.,* 2011]. The transpressive kinematics of the WISZ [*McClelland et al.,* 2000] suggest that contractional strain might have been accommodated across a region wider than the narrow (<10 km) shear zone. A recent study [*Davis and Giorgis*, 2014] estimates that the shortening across the WISZ is at most 5 km. Overall, questions remain about what structures, in addition to the WISZ, accommodated dextral strike-slip motion and the margin-normal contractional strain in the northern U.S. Cordillera and when these structures developed. This work addresses some of these questions by investigations of an area about 90 km east of the WISZ utilizing structural and zircon U-Pb data from metasedimentary and intrusive rocks in the Sawtooth metamorphic complex, Idaho.

2. Geologic Background

To the west of the Cretaceous-Paleogene Idaho batholith, largely in northeastern Oregon, the Blue Mountains province comprises an island arc (Wallowa terrane), a subduction-accretionary complex (Baker terrane), an arc-related basin (Izee terrane), and a continent-fringing arc (Olds Ferry terrane) (Figure 1a) [e.g., *Burchfiel et al.,* 1992; *Vallier*, 1995; *Gray and Oldow*, 2005; *Dorsey and LaMaskin*, 2007; *LaMaskin et al.,* 2011, 2015]. The Wallowa terrane consists of Paleozoic and Mesozoic volcanic rocks formed offshore as an intra-oceanic arc [e.g., *Vallier*, 1995; *Dorsey and LaMaskin*, 2007]. Accretion of the Blue Mountains to the North American craton occurred mostly during Late Triassic to Late Jurassic time, and the subsequent deformation continued into the Early Cretaceous [e.g., *Selverstone et al.,* 1992; *Getty et al.,* 1993; *Dorsey and LaMaskin*, 2007; *LaMaskin et al.,* 2011, 2015]. The Blue Mountains province is separated from the North American craton to the east by the 25–35 km wide Salmon River suture zone [e.g., *Manduca et al.,* 1993; *Gray and Oldow*, 2005]

19449194, 2017, 3, Downloaded from https://agupubs.onlinelibrary.wiley.com/doi/10.1002/2016TC004264 by Auburn University Libraries, Wiley Online Library on [27/10/2022]. See the Terms and Conditions (https://onlinelibrary.wiley.com/terms-and-conditions) on Wiley Online Library for rules of use; OA articles are governed by the applicable Creative Commons License

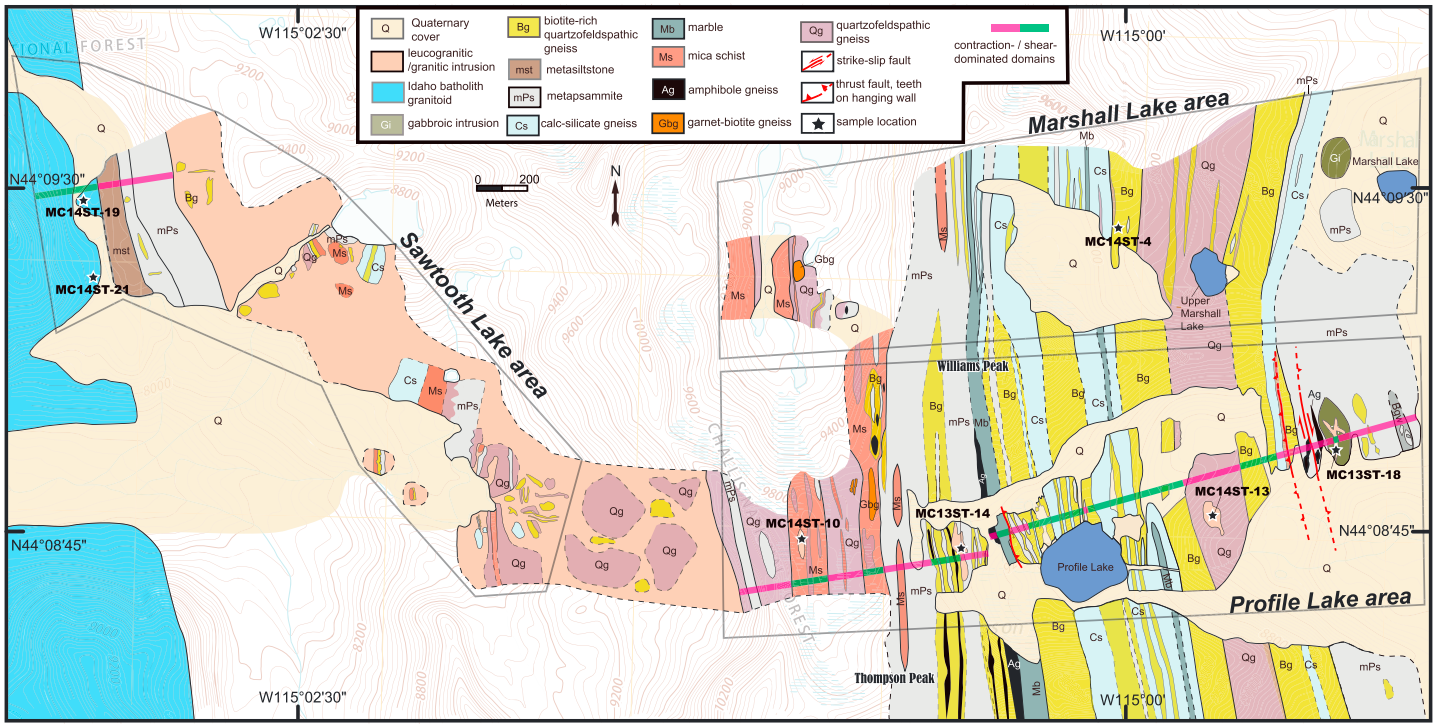

Figure 2. Generalized geologic map of the Sawtooth metamorphic complex showing lithology units and sample locations. See the box in Figure 1b for map location. The three polygons represent the three areas where the structural data in Figure 3 were collected. Note that the shear- and contraction-dominated domains are only generally distinguished, and they could be further discriminated within each domain on the current map.

that formed in Early Cretaceous time due to the final docking of the Blue Mountains composite terrane [*Getty et al.,* 1993; *Tikoff et al.,* 2001]. Within this suture zone, a narrow (<10 km) midcrustal exposure of lithospheric-scale shear zone, WISZ, records both dextral and contractional Late Cretaceous deformations [e.g., *McClelland et al.,* 2000; *Giorgis et al.,* 2008; *Blake et al.,* 2009].

The WISZ is defined by penetrative strained fabrics in a north-south-striking linear zone of coarse-grained tonalite, quartz diorite, and porphyritic orthogneisses on the western edge of the Idaho batholith [*Manduca et al.,* 1993; *Giorgis et al.,* 2008]. Mylonitic foliations, defined by planarly distributed minerals, strike north-south and dip steeply to the east; stretching lineations, defined by biotite trails, elongate quartz grains, and other oriented minerals, plunge subvertically in the foliation plane [e.g., *Lund and Snee*, 1988; *Manduca et al.,* 1993]. Centimeter- to meter-scale tight folds in the WISZ are characterized by parallel-to-the-surrounding-foliation axial planes and steeply plunging fold axes [*Manduca et al.,* 1993; *Blake et al.,* 2009]. Kinematic indicators in the movement plane do not show a consistent sense of shearing, but a dextral sense of shear is generally concluded [e.g., *Lund and Snee*, 1988; *Manduca et al.,* 1993; *Giorgis et al.,* 2008]. The main phase deformation of the WISZ occurred between ca. 105 Ma and ca. 90 Ma, and the late-stage deformation on the zone is bracketed between ca. 90 Ma and ca. 80 Ma on the basis of zircon U-Pb data and biotite/hornblende $^{40}Ar/^{39}Ar$ data, respectively [*Giorgis et al.,* 2008]. Many studies propose that the WISZ has accommodated juxtaposition and northward translation of the Blue Mountains province in Cretaceous time by various amounts of dextral strike-slip motion, ranging from less than 100 km [e.g., *Saleeby and Busby-Spera*, 1992; *Dickinson*, 2004] to ~400 km [e.g., *Wyld and Wright*, 2001; *Wright and Wyld*, 2007] to >1000 km [e.g., *Housen and Dorsey*, 2005]. On the basis of U-Pb data of detrital zircons from the Izee terrane and Olds Ferry terrane strata, *LaMaskin et al.* [2011] support a ~400 km-scale northward translation of the Blue Mountains along the WISZ. These variable estimates suggest that additional structures may have accommodated northward motion of the accreted terranes.

The Sawtooth metamorphic complex (SMC), Idaho, is an isolated exposure of predominantly high-grade metasedimentary rocks within the Idaho batholith [*Dutrow et al*., 2014]. Rocks of the SMC are in rare intrusive contact with Cretaceous granitoids of the Atlanta lobe of the Idaho batholith along the western and southern

19449194, 2017, 3, Downloaded from https://agupubs.onlinelibrary.wiley.com/doi/10.1002/2016TC004264 by Auburn University Libraries, Wiley Online Library on [27/10/2022]. See the Terms and Conditions (https://onlinelibrary.wiley.com/terms-and-conditions) on Wiley Online Library for rules of use; OA articles are governed by the applicable Creative Commons License

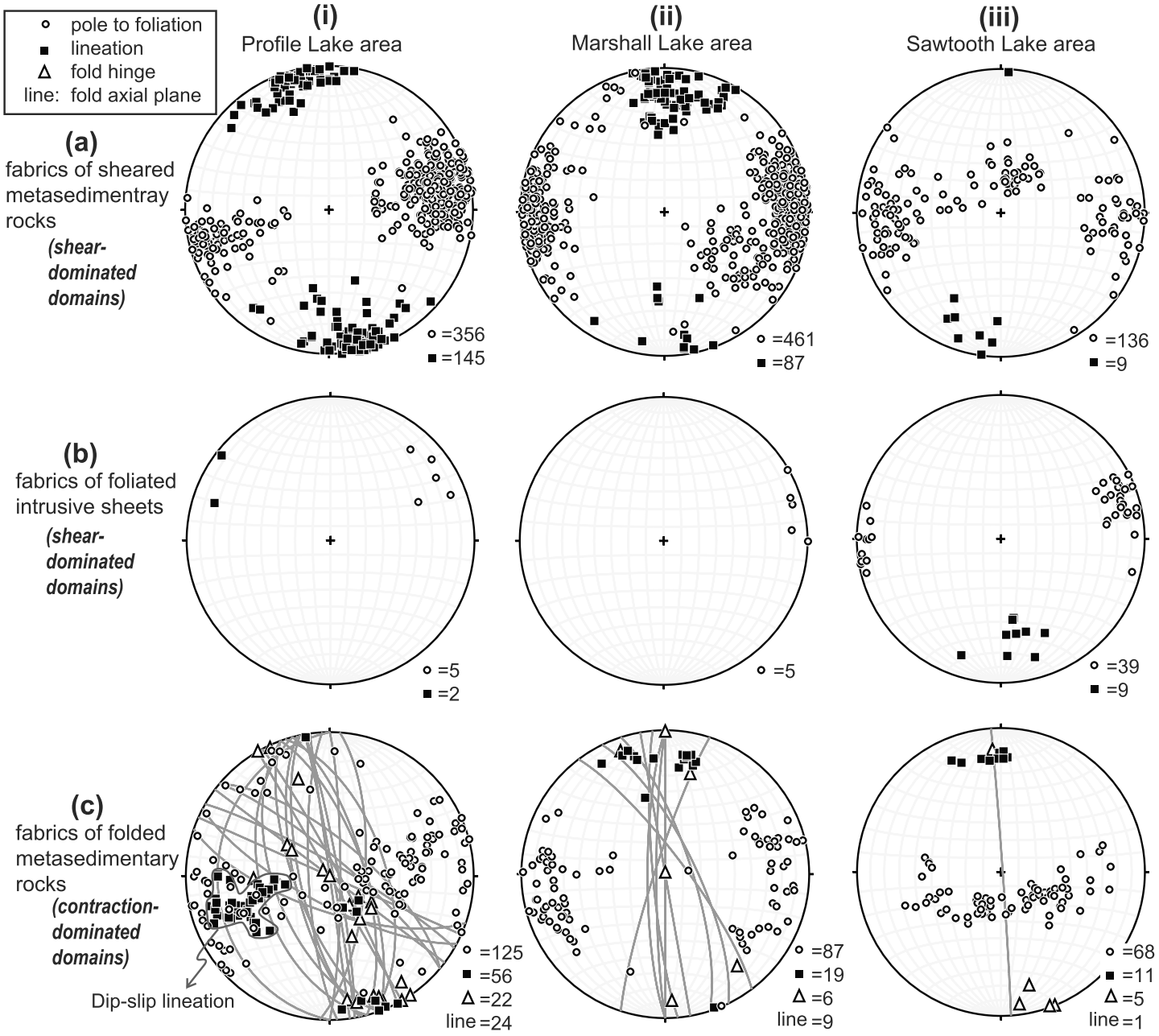

Figure 3. Structural data of the Sawtooth metamorphic complex. See Figure 2 for locations of the Profile Lake, Marshall Lake, and Sawtooth Lake areas.

margins and interpreted to be in contact with the Eocene Sawtooth batholith along the northern margin. The SMC is bounded on the east side by a buried east-dipping normal fault (Figure 1b) [*Reid*, 1963; *Fisher et al.,* 1992; *Dutrow et al.,* 1995]. The SMC metasedimentary rocks are mostly composed of intermediate- to high-grade siliciclastic and carbonate materials (Figure 2) [*Dutrow et al.,* 1995; *Metz*, 2010; *Fukai*, 2013; *Ma*, 2015], the protoliths of which were likely deposited in the Cambrian and Middle Ordovician [*Ma et al.,* 2016]. These metasedimentary rocks are intruded by gabbroic, granitic, and leucogranitic sheets, pods, and dikes, along with Eocene Challis rhyolitic and basaltic dikes [e.g., *Ma*, 2015].

3. Structures

The most noticeable deformational features of the SMC are subvertical compositional layers [*Metz*, 2010; *Bergeron*, 2012] resulting in an elongate map pattern of transposed lithologic units (Figure 2) and a

19449194, 2017, 3, Downloaded from https://agupubs.onlinelibrary.wiley.com/doi/10.1002/2016TC004264 by Auburn University Libraries, Wiley Online Library on [27/10/2022]. See the Terms and Conditions (https://onlinelibrary.wiley.com/terms-and-conditions) on Wiley Online Library for rules of use; OA articles are governed by the applicable Creative Commons License

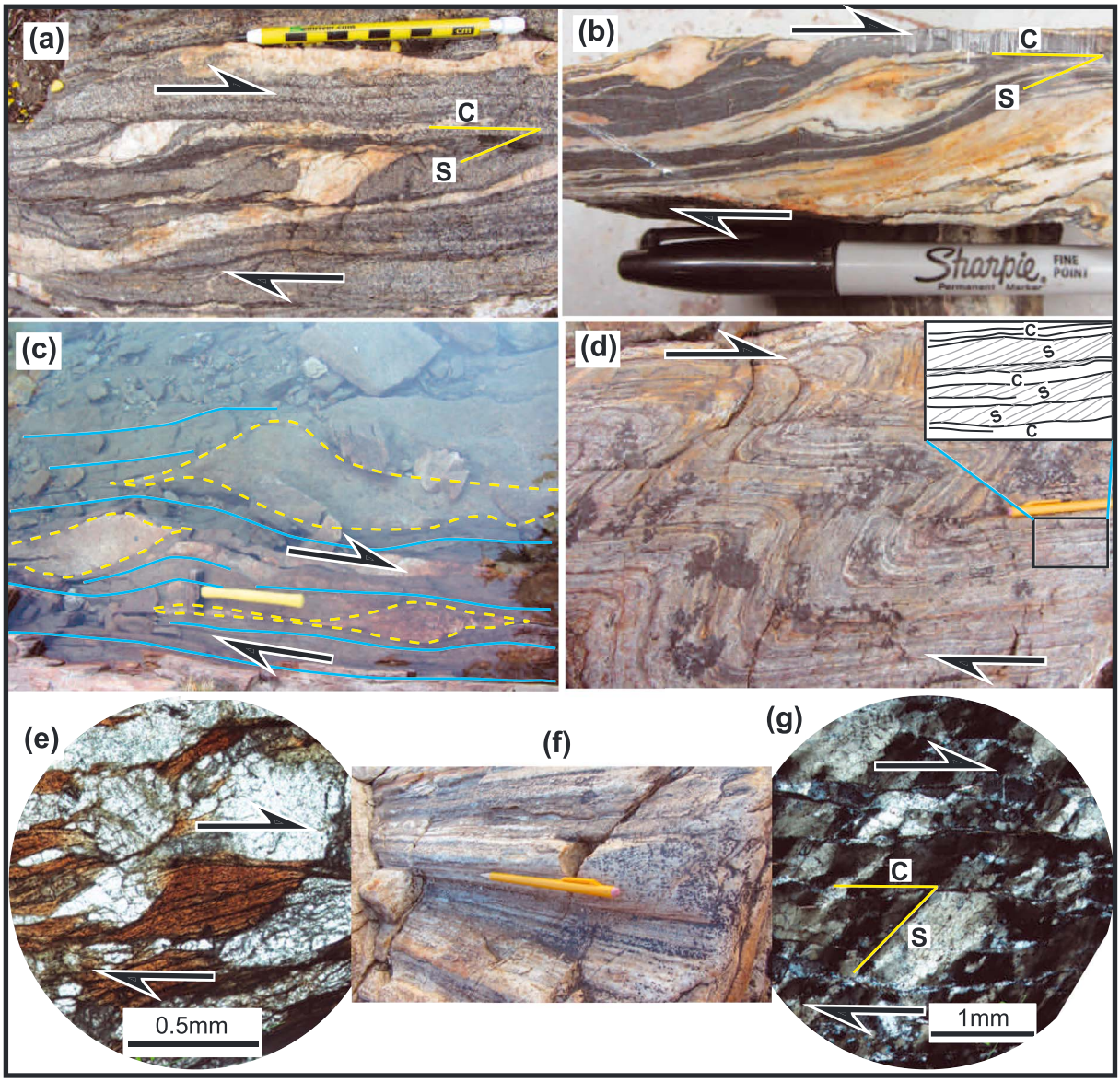

Figure 4. Representative structures in shear-dominated domains. (a) Sigma-type porphyroclasts and S-C fabrics; (b) delta-type porphyroclasts and S-C fabrics; (c) asymmetric boudinaged metapsammite blocks; (d) asymmetric folds with pervasive S-C fabrics in their limbs; (e) mica fish; (f) subhorizontal strike-slip lineations on a folded surface; (g) S-C fabrics defined by oriented biotite and quartz lattice (displaying preferred orientation of extinction simultaneously) in quartzofeldspathic gneiss. Notes: pens (~13 cm) and hammer (~35 cm) for scales; view southwest in Figure 4f; view down in Figures 4a–4g in which the right side of the photo points to the north; arrows indicate dextral sense of shear.

heterogeneous deformational pattern at the mesoscale. Deformation transposed lithologic layers to produce pervasive foliation parallel to the compositional layers. It is unclear whether the gross compositional layering reflects primary sedimentary units or resulted largely from metamorphic differentiation and transposition. Locally, however, some primary sedimentary contacts and structures are observed in moderately strained zones, and these are parallel to the compositional layers.

Most of the SMC rocks contain steeply dipping foliation and subhorizontal lineation (Figure 3). General orientation of foliation and lineation varies slightly along-strike from N-S in the Marshall Lake area to NNW-SSE in the Profile Lake area (Figures 3a, 3b, and 3c, stereoplots i and ii). The relatively diffuse distribution of poles to foliation in the Sawtooth Lake area (Figure 3a, stereoplot iii) is likely due to the disturbance by pervasive intrusion of the Idaho leucogranite in the eastern portion of this area where it is dominated by intrusive rocks (Figure 2). Fabrics in the western Sawtooth Lake area near the Idaho batholith, however, share common

19449194, 2017, 3, Downloaded from https://agupubs.onlinelibrary.wiley.com/doi/10.1002/2016TC004264 by Auburn University Libraries, Wiley Online Library on [27/10/2022]. See the Terms and Conditions (https://onlinelibrary.wiley.com/terms-and-conditions) on Wiley Online Library for rules of use; OA articles are governed by the applicable Creative Commons License

orientations with the fabrics in the eastern SMC (Figure 3b, stereoplot iii). The following descriptions and later discussions of structural fabrics are based on data collected from the Profile Lake area, Marshall Lake area, and the western Sawtooth Lake area (Figure 2).

Structural fabrics in the SMC vary gradually across strike between two types of deformational domains that share a common orientation: centimeter-wide to several hundred meter-wide domains of shear-dominated fabrics and meter-wide to several hundred meter-wide domains of contraction-dominated fabrics. The shear-dominated domains are generally defined by foliated granitic intrusions and rheologically weak lithologies, e.g., mica schist, marble, calc-silicate gneiss, and biotite-rich quartzofeldspathic gneiss. The contraction-dominated domains are normally defined by mica-poor quartzofeldspathic gneiss and metapsammite. These two types of domains are generally distinguished on Figure 2.

3.1. Shear Zones

The SMC shear zones consist of metasedimentary rocks (dominantly marble, mica schist, calc-silicate gneiss, and biotite-rich quartzofeldspathic gneiss) and felsic intrusive sheets. Mylonitic foliations in shear zones strike N-S to NNW-SSE and dip steeply to either east or west; strike-slip lineations plunge subhorizontally shallowly to either north or south (Figures 3a and 3b, stereoplots i–iii).

3.1.1. Fabrics in Metasedimentary Rocks

Well-developed kinematic indicators in the shear zones occur on the plane perpendicular to foliation and parallel to lineation in the metasedimentary rocks, and they consistently indicate a dextral strike-slip motion. At the mesoscale, sigma-porphyroclasts, delta-porphyroclasts, S-C fabrics, and 0.5–1 m boudinaged metapsammite blocks (Figures 4a, 4b, and 4c) show dextral sense of shearing. Asymmetric folds also occur widely on the movement plane and contain pervasive S-C fabrics on their limbs (Figure 4d), both of which reveal dextral sense of shearing. Based on the profile geometry of the asymmetric folds on the movement plane of shearing, most of the asymmetric folds are characteristic of similar folds. Dextral strike-slip shearing is also revealed by microstructures such as mica fish in biotite-rich quartzofeldspathic gneiss (Figure 4e) and S-C fabrics represented by oriented quartz (displaying preferred orientation of extinction simultaneously) and foliated biotite in metapsammite (Figure 4g). The strike-slip shearing is significant as evidenced by well-developed subhorizontal mineral stretching lineations (Figure 4f).

Sheath folds locally occur in the cross-section exposure perpendicular to the strike-slip lineations. For example, in a mylonitic shear zone that largely consists of gray marble, quartzofeldspathic gneiss, and calc-silicate gneiss with strong dextral shear fabrics on the subhorizontal surface (Figure 5a), sheath folds are exposed in the cross section that provides a transport-normal view (Figure 5b). These sheath folds have hinge-line curvatures varying from $>90°$ (Figure 5c) to $>160°$ (i.e., tubular folds, Figure 5d). Overall, the fabrics and structures in the shear zones are consistent with those being dominated by wrench faulting with significant strain.

3.1.2. Fabrics in Felsic Intrusive Sheets

Felsic intrusives with magmatic foliations are common in the shear zones. These magmatically deformed intrusions share foliation and lineation orientations with the surrounding metasedimentary rocks (Figure 3b, stereoplots i–iii), which are distinguished from those younger intrusions that crosscut the metasedimentary rocks and generally do not show any foliation. These magmatically foliated intrusions, cropping out as intrusive sheets, are granitic and have widths that vary from a few centimeters to several tens of meters. Strong magmatic foliations are defined by feldspar augens (Figure 6a), gneissic xenoliths (Figure 6b), and mafic minerals (mostly biotite) (Figure 6e). Winged porphyroclasts and S-C fabrics (e.g., Figures 6c and 6d) in the intrusive sheets indicate dextral strike-slip shearing. Microscopic examination of orientated samples from magmatically foliated intrusive sheets shows that quartz, feldspar, and mica are not deformed (e.g., Figures 7a and 7b) and, in most cases, biotite is strongly to weakly (Figures 7c and 7d) aligned along north-south parallel to the foliations of the surrounding metasedimentary rocks. The magmatic foliations in those felsic intrusive sheets therefore indicate that deformation was ongoing when the material was dominated by crystals with a lesser fraction of melt. This feature is distinguished from the formation of mylonitic foliations in the metasedimentary rocks that were deformed in solid state.

3.2. Contraction-Dominated Domains

Structures in metasedimentary rocks (largely quartzofeldspathic gneiss and metapsammite) outside of the shear zones are dominated by folds. Magmatically foliated felsic intrusions are generally not present

19449194, 2017, 3, Downloaded from https://agupubs.onlinelibrary.wiley.com/doi/10.1002/2016TC004264 by Auburn University Libraries, Wiley Online Library on [27/10/2022]. See the Terms and Conditions (https://onlinelibrary.wiley.com/terms-and-conditions) on Wiley Online Library for rules of use; OA articles are governed by the applicable Creative Commons License

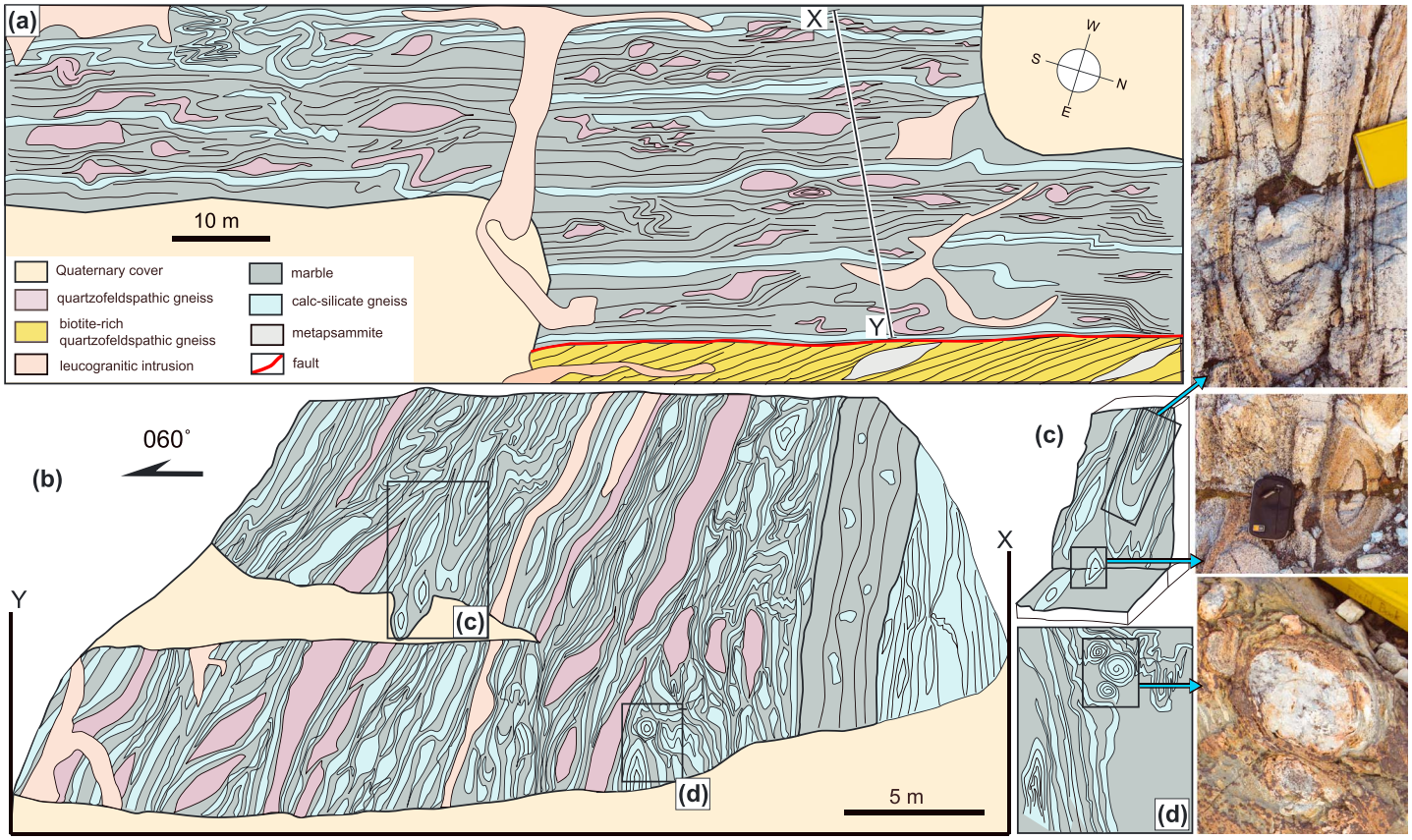

Figure 5. Mylonitic shear zone composed by gray marble, quartzofeldspathic gneiss, and calc-silicate gneiss. (a) Subhorizontal exposure; (b) cross section, see line XY in Figure 5a for projected location; (c) three-dimensional exposure of sheath folds and steeply plunged folds; (d) exposure of tubular folds. See boxes in Figure 5b for locations of Figures 5c and 5d. Notebook and camera bag (~11 cm) for scales.

outside of the shear zones. The contraction-dominated domains are characterized by roughly north-south-trending folds (Figures 3c, stereoplots i–iii, 8a, and 8b) and thrusts (Figures 8d and 8e).

The scale of the folds varies from >100 m (Figure 8a) to a few centimeters (Figure 8b). Most of the folded lithologic layers share a common north-south strike. The dips, however, vary from subvertical to subhorizontal and mostly have steep angles dipping to either east or west (Figure 3c, stereoplots i–iii). Axial planes are primarily subvertical to steep with north-south strikes, although some strike northwesterly in the Profile Lake area (Figure 3c, stereoplot i). Interlimb angles vary from about 0° to 90°, indicating developments of isoclinal, tight, closed, and open folds. The isoclinal and tight folds occur mainly in less competent rocks, e.g., interlayered marble and calc-silicate gneiss, while most of the closed and open folds occur in relatively competent rocks, e.g., quartzofeldspathic gneiss and metapsammite. Fold hinges plunge shallowly to steeply to either north or south (Figure 3c, stereoplots i–iii). Various plunges of fold hinges suggest that the SMC folds are markedly curvilinear. There are two kinds of lineations on the folded surface: north-south-trending, subhorizontal to shallow-plunging lineations (Figure 3c, stereoplots i–iii) parallel to the strike-slip lineations in the shear-dominated domains, and E-W- to NE-SW-trending, shallow-to-steep-plunging dip-slip lineations (Figures 8c and 3c, stereoplot i) roughly orthogonal to the strike-slip lineations in the shear-dominated domains. The former lineation is defined largely by quartz ribbons and is predominant in the study area. The later lineation is defined by quartz slickenfibers and ridge-in-groove structures and is only locally preserved on meter-scale outcrops.

Thrust faults are kinematically and spatially associated with folds in the contraction-dominated domains. Centimeter-scale thrust faults occur in individual layers with small displacements, and are genetically related to the parasitic folds of the same outcrop (Figure 8d). Meter-scale thrust faults cut multiple layers and form ramps and flats that facilitated development of fault-propagation folds (Figure 8e). Geometry of larger thrusts (tens of meter scale) is less clear although the exposed segments of fault planes are relatively

19449194, 2017, 3, Downloaded from https://agupubs.onlinelibrary.wiley.com/doi/10.1002/2016TC004264 by Auburn University Libraries, Wiley Online Library on [27/10/2022]. See the Terms and Conditions (https://onlinelibrary.wiley.com/terms-and-conditions) on Wiley Online Library for rules of use; OA articles are governed by the applicable Creative Commons License

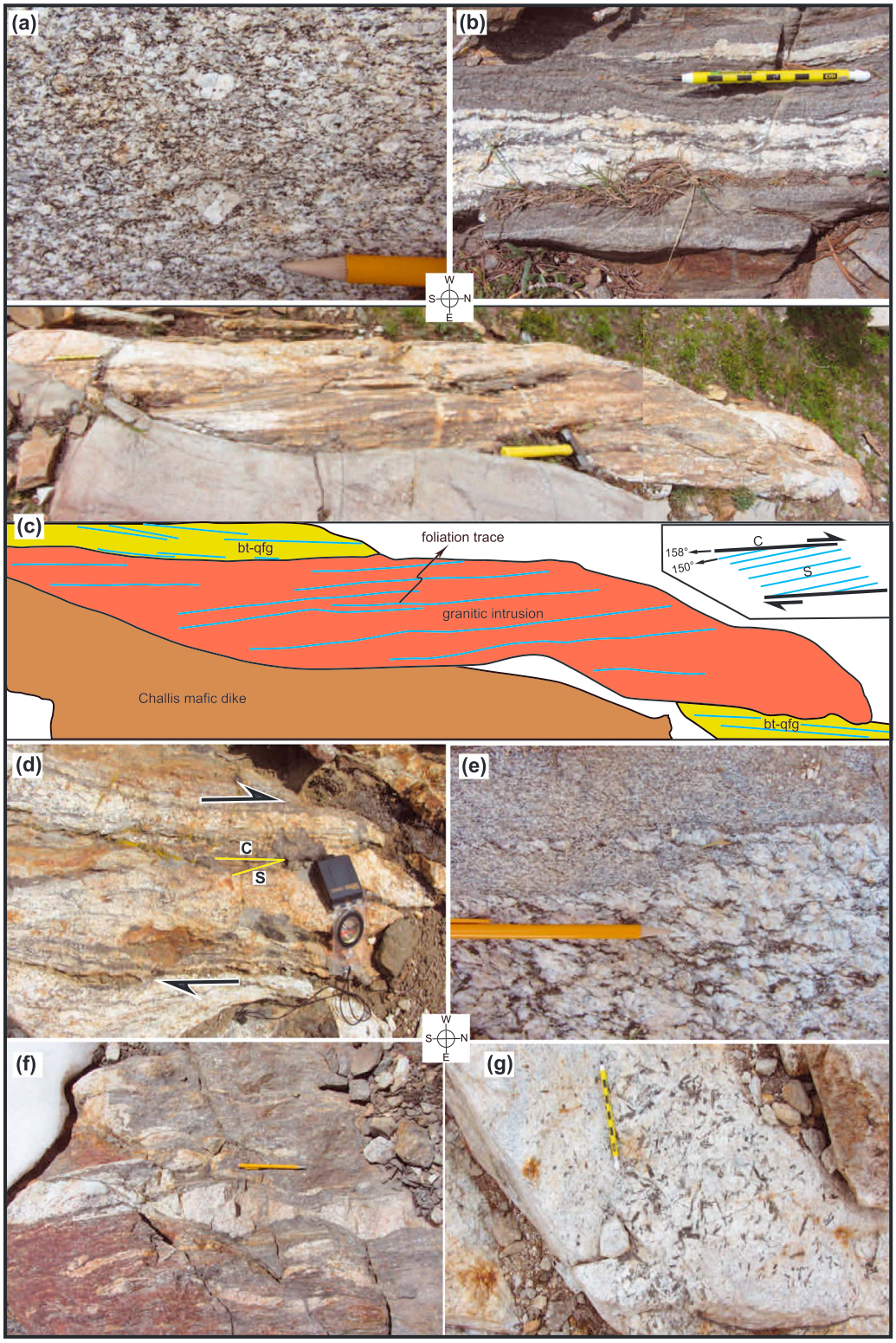

Figure 6. Outcrops of intrusive sheets (a–e) with and (f–g) without magmatic foliations. (a) Outcrop for sample MC14ST-21; (b) outcrop for sample MC14ST-4; (c) magmatically foliated intrusion showing S-C structures; (d) outcrop for sample MC13ST-18, note the S-C fabrics of magmatic foliation defined by biotite layers; (e) outcrop for sample MC14ST-13, note the concordant apophysis of the intrusion; (f) outcrop for sample MC14ST-10, note the absence of pervasive foliation in the intrusion; (g) pegmatitic biotite leucogranite. All pictures are viewed from above; the right side of each photo points to the north; kinematic indicators of dextral sense of shear are available on the outcrop for all the magmatically foliated intrusive sheets (Figures 6a–6e). bt-qfg = biotite-rich quartzofeldspathic gneiss. Pens, hammer, and compass for scales.

19449194, 2017, 3, Downloaded from https://agupubs.onlinelibrary.wiley.com/doi/10.1002/2016TC004264 by Auburn University Libraries, Wiley Online Library on [27/10/2022]. See the Terms and Conditions (https://onlinelibrary.wiley.com/terms-and-conditions) on Wiley Online Library for rules of use; OA articles are governed by the applicable Creative Commons License

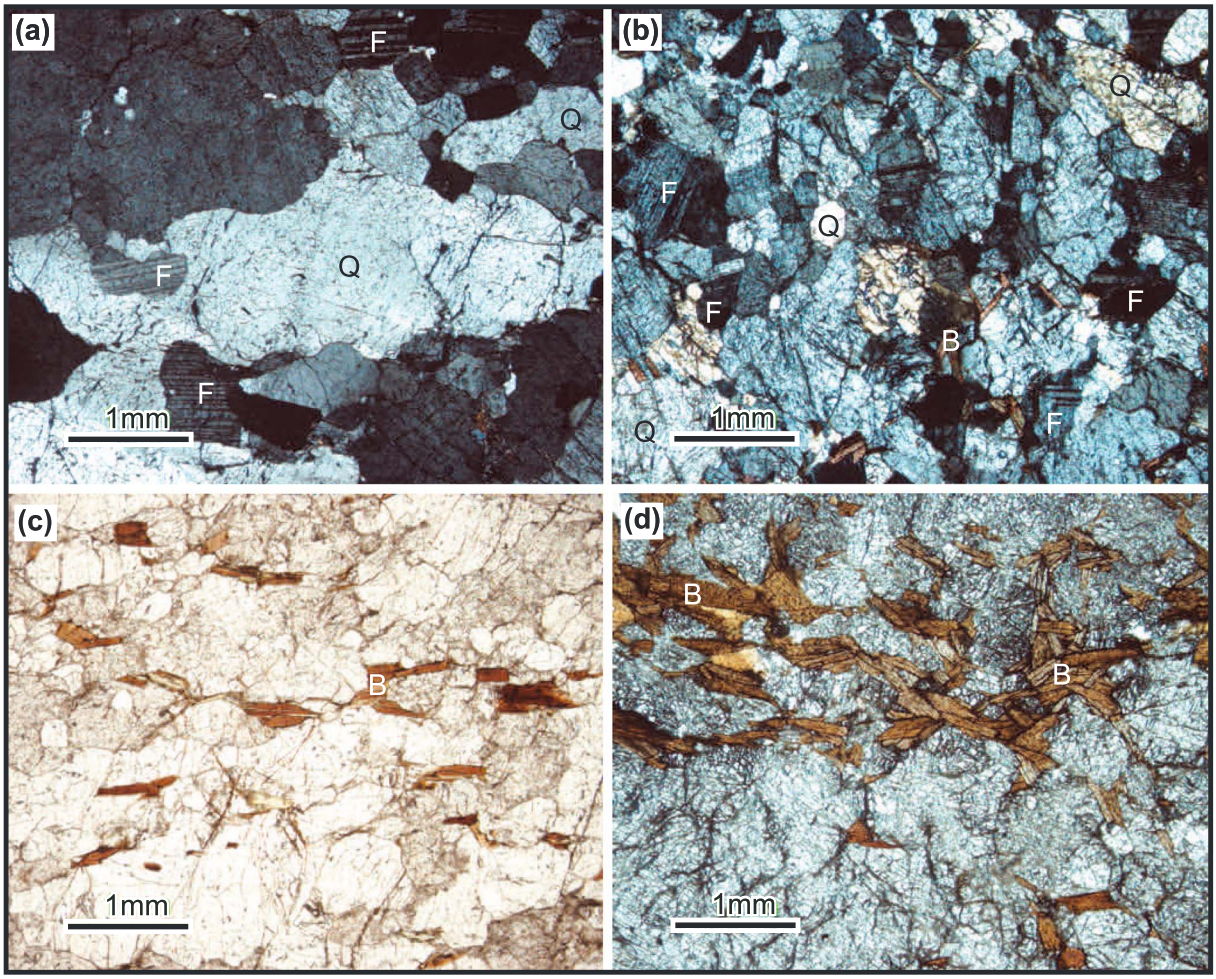

Figure 7. Representative photomicrographs of magmatically foliated intrusive sheets in the shear-dominated domains. (a) Coarse- and (b) medium-grained quartz and feldspar show no deformation (cross-polarized light); (c) sparse and (d) abundant euhedral biotite aligns along north-south defining the magmatic foliation (plane-polarized light). B = biotite, F = feldspar, Q = quartz.

even (e.g., Figure 8f). Fault kinematics was determined in the field primarily based on the asymmetry of fault-propagation folds (e.g., Figures 8d and 8e) and secondary drag folds (e.g., Figure 8f). Most fault planes are roughly north-south striking with moderate eastward or westward dips. An undeformed leucogranite dike crosscutting a thrust fault shows that intrusion continued after shortening in this area (Figure 8f).

3.3. Transitional Structures

In contraction-dominated domains, strong subhorizontal stretching lineations on folded surfaces indicate a strike-slip component to the overall strain. In shear-dominated domains, a variety of contraction structures are locally developed. Isoclinally folded quartzofeldspathic layers (Figures 9a and 9b) are preserved in rootless structures within the marble shear zones (Figure 5b). The hinges of those rootless isoclinal folds are parallel to the subhorizontal lineation of the host shear zone, and the fold axial planes are parallel to the shear plane, indicating transposition of folds by strike-slip shearing. In cross section (Figures 5b), hinge zones pointing upward (see the arrow in Figure 9a) or downward (see the arrow in Figure 9b) indicate vertical movements. In the same cross section (Figure 5b), boudinaged quartzofeldspathic blocks are arranged into S-C structures showing east-up-and-west-down (Figure 9c) or east-down-and-west-up (Figure 9d) vertical movements.

Crosscutting relationships rarely exists between shear zones and folds. Only two outcrops containing cross-cutting structures were observed, and they show different relationships due to progressive deformation. In one outcrop of folds (Figure 10a), a ~20 cm wide shear zone with strong mylonitic fabrics (Figure 10b) cross-cuts one side of the folds but not the other, which suggests that shearing started after or during folding. In

19449194, 2017, 3, Downloaded from https://agupubs.onlinelibrary.wiley.com/doi/10.1002/2016TC004264 by Auburn University Libraries, Wiley Online Library on [27/10/2022]. See the Terms and Conditions (https://onlinelibrary.wiley.com/terms-and-conditions) on Wiley Online Library for rules of use; OA articles are governed by the applicable Creative Commons License

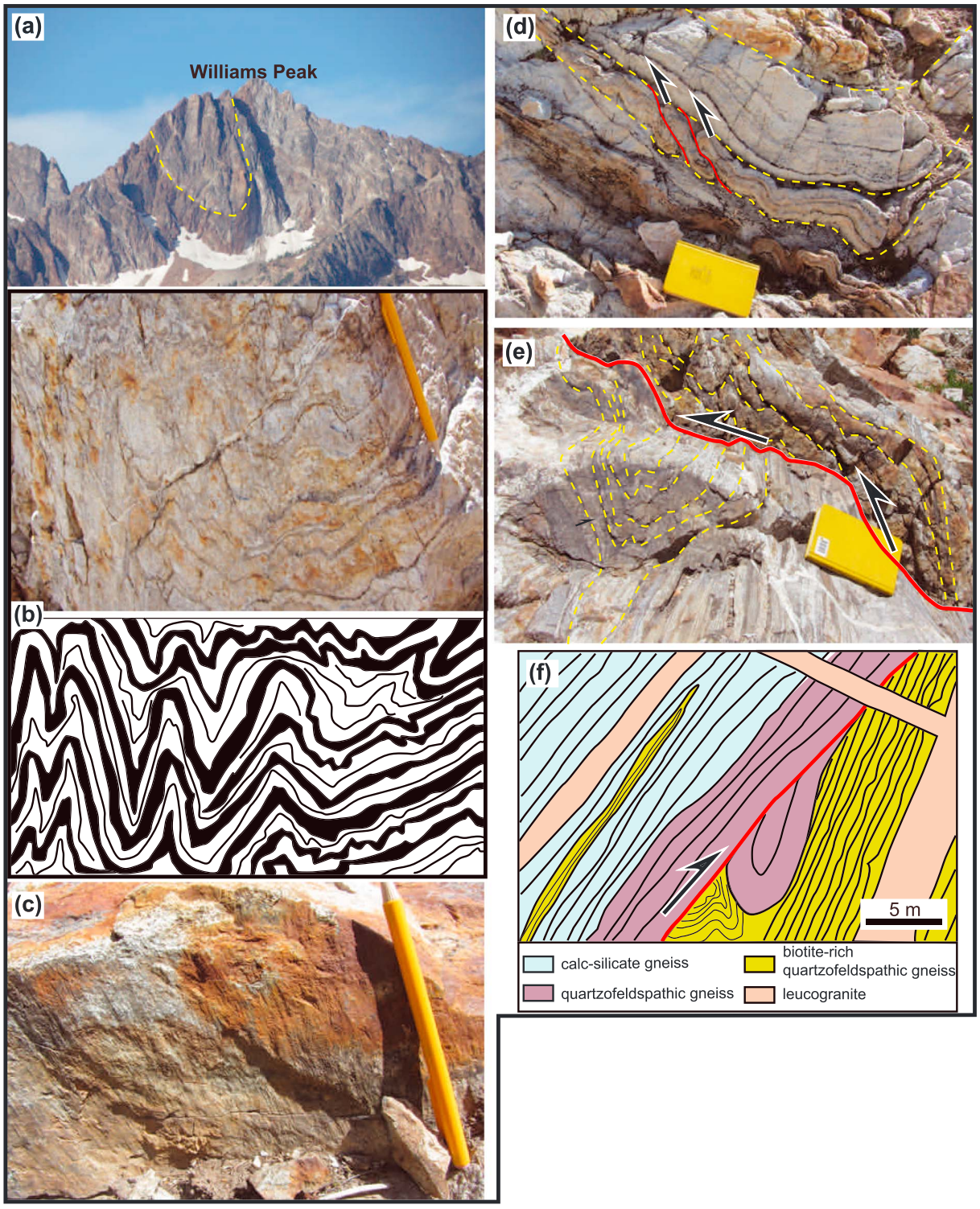

Figure 8. Representative structures in the contraction-dominated domains. (a) A large (>100 m) fold exposed on the Williams ridge defined by contact (see the dashed line) between biotite-rich quartzofeldspathic gneiss and calc-silicate gneiss, view to the southwest; (b) small (centimeter-scale) folds defined by folded biotite-rich layers (black strips in the sketch), view south; (c) steep dip-slip lineations on a folded surface; (d) parasitic folds with associated centimeter-scale thrust faults, view south; (e) a meter-scale thrust fault with fault-propagation folds above, view north; (f) sketch of a tens of meter-scale thrust fault that cut by a leucogranite dike, view north.

19449194, 2017, 3, Downloaded from https://agupubs.onlinelibrary.wiley.com/doi/10.1002/2016TC004264 by Auburn University Libraries, Wiley Online Library on [27/10/2022]. See the Terms and Conditions (https://onlinelibrary.wiley.com/terms-and-conditions) on Wiley Online Library for rules of use; OA articles are governed by the applicable Creative Commons License

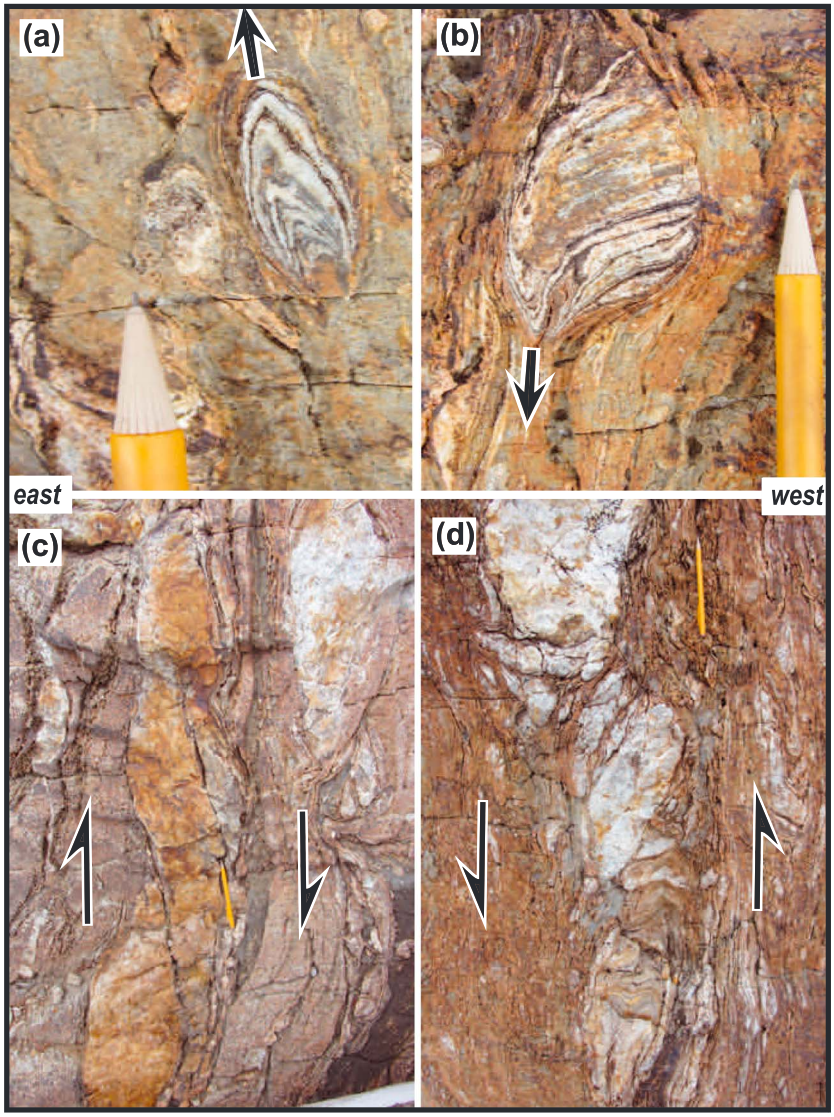

Figure 9. Structures in cross sections showing the vertical lengthening component of transpression in the Sawtooth metamorphic complex. Isoclinal folds of quartzofeldspathic layers folded (a) upward and (b) downward; S-C structures defined by boudinaged quartzofeldspathic blocks showing (c) east-up-and-west-down and (d) west-up-and-east-down movements. All photos are viewed south. Pencil for scale.

another outcrop, mylonitic fabrics are folded into a north-south-striking, tight-isoclinal folds (Figure 10c). In contrast to the dominant dextrally sheared porphyroclasts across the study area, sigma-porphyroclasts indicative of sinistral shearing occur on one side of the folds (Figure 10c). Folded mylonitic fabrics and opposite kinematic indicators across the folds suggest that folding took place after shearing. Some ductilely disturbed segments and uneven thickness of folded layers (see the lower part of Figure 10c) indicate that there was a minor strike-slip movement during folding. For the two outcrops described above, the sheared and folded fabrics have generally similar orientations to that of the SMC shear- and contraction-dominated domains.

4. Zircon U-Pb Geochronology

4.1. Methods

Unweathered samples of granitic/leucogranitic rocks were crushed, milled, and sieved prior to zircon separation using traditional magnetic and density-based methods followed by handpicking under a binocular

19449194, 2017, 3, Downloaded from https://agupubs.onlinelibrary.wiley.com/doi/10.1002/2016TC004264 by Auburn University Libraries, Wiley Online Library on [27/10/2022]. See the Terms and Conditions (https://onlinelibrary.wiley.com/terms-and-conditions) on Wiley Online Library for rules of use; OA articles are governed by the applicable Creative Commons License

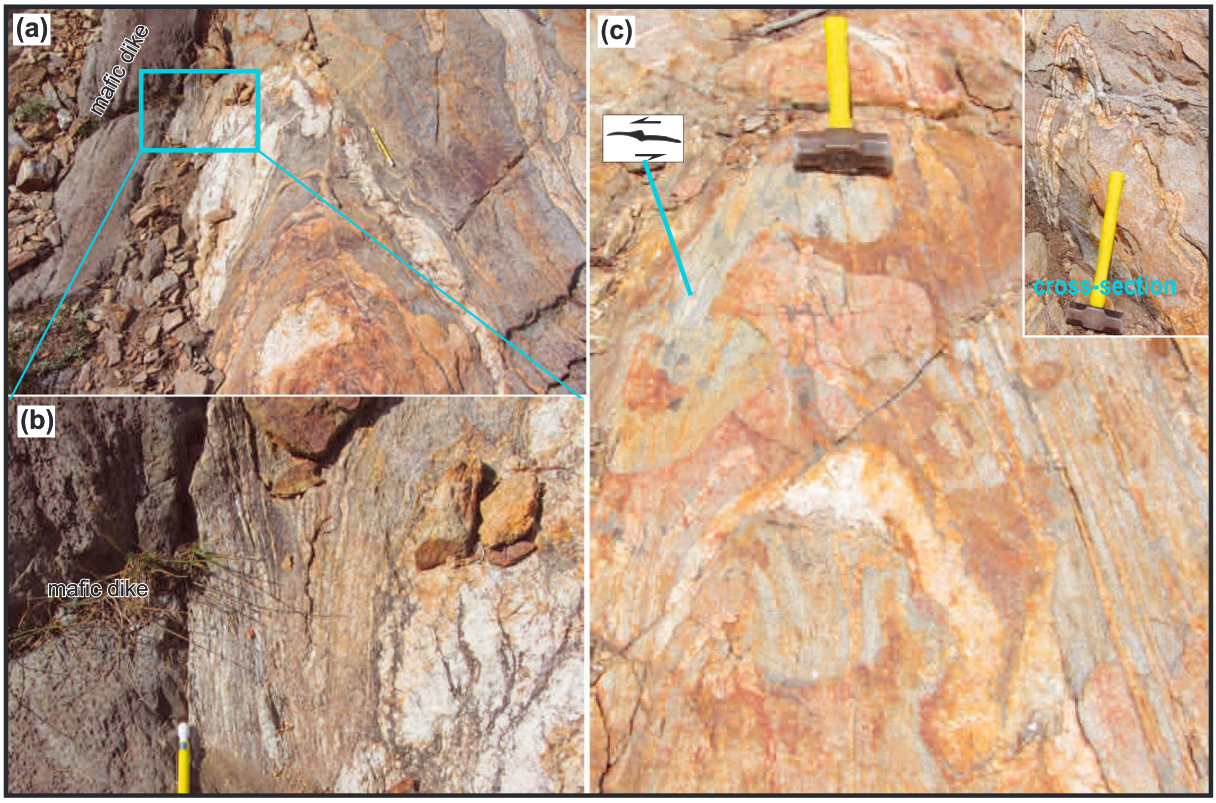

Figure 10. Mutually crosscutting relationships between sheared fabrics and folded structures. (a, b) A ~20 cm wide shear zone crosscuts one side limbs of a suite of folds whereas the other side limbs are lacking of sheared fabrics. Note that the mafic dike on the left is a younger intrusion and was not a boundary for localizing shearing during the development of the shear zone. (c) Sheared fabrics have been folded exposing on a subhorizontal surface; inset is a cross-sectional view; note the winged porphyroclast showing sinistral shearing in one of the left side limbs. Pencil and hammer for scales.

microscope. The zircon grains were mounted in epoxy and polished to expose cross sections, which were imaged using cathodoluminescence and backscattered electrons with a Zeiss scanning electron microscope at the University of Florida to identify internal structures (i.e., cores and rims) and compositional variations (i.e., zoning). U-Pb isotopic analyses were performed on a Nu-Plasma multicollector inductively coupled plasma mass spectrometer integrated with a New Wave 213 nm ultraviolet Nd:YAG laser ablation system at the University of Florida following *Mueller et al.* [2008]. FC-1 zircon from the Duluth Complex with an age of 1099.0 ± 0.6 Ma [*Paces and Miller*, 1993; *Black et al.,* 2003; *Mattinson*, 2010] was used as the primary age reference for data calibration and drift correction. R33 zircons from the Braintree Complex with an age of 419.26 ± 0.39 Ma [*Black et al.,* 2004] were run as the secondary standard (Table S2 in the supporting information). Two FC-1 zircons were analyzed after every 10 unknowns. Both standards and unknowns were ablated for 30 s (300 laser shots) with identical laser and mass spectrometer parameters. Drift corrections were made by linear bracketing with the FC-1 standards. Data were reduced using an in-house Excel spreadsheet and plotted using Isoplot [*Ludwig*, 2012]. Because some zircons analyzed have exhibited slight inheritance or Pb loss, the TuffZirc algorithm of Isoplot was utilized to extract reliable ages [*Ludwig*, 2012]. The TuffZirc algorithm calculates a median age of the largest coherent (statistically within analytical error) group of zircons and interprets it as the best estimation of the true age with an asymmetric uncertainty derived from the 95% confidence errors of the median age [*Ludwig*, 2012]. Full tabulations of the coordinates of sample locations and U-Pb isotopic data are included in Tables S1 and S2, respectively.

4.2. Results

Seven felsic igneous samples comprising five magmatically foliated (Figure 11) and two unfoliated (Figure 12) intrusions were collected from different areas in the SMC for U-Pb geochronology (see Figure 2 for sample locations). The zircons analyzed are mostly euhedral and show oscillatory zoning typical of magmatic

19449194, 2017, 3, Downloaded from https://agupubs.onlinelibrary.wiley.com/doi/10.1002/2016TC004264 by Auburn University Libraries, Wiley Online Library on [27/10/2022]. See the Terms and Conditions (https://onlinelibrary.wiley.com/terms-and-conditions) on Wiley Online Library for rules of use; OA articles are governed by the applicable Creative Commons License

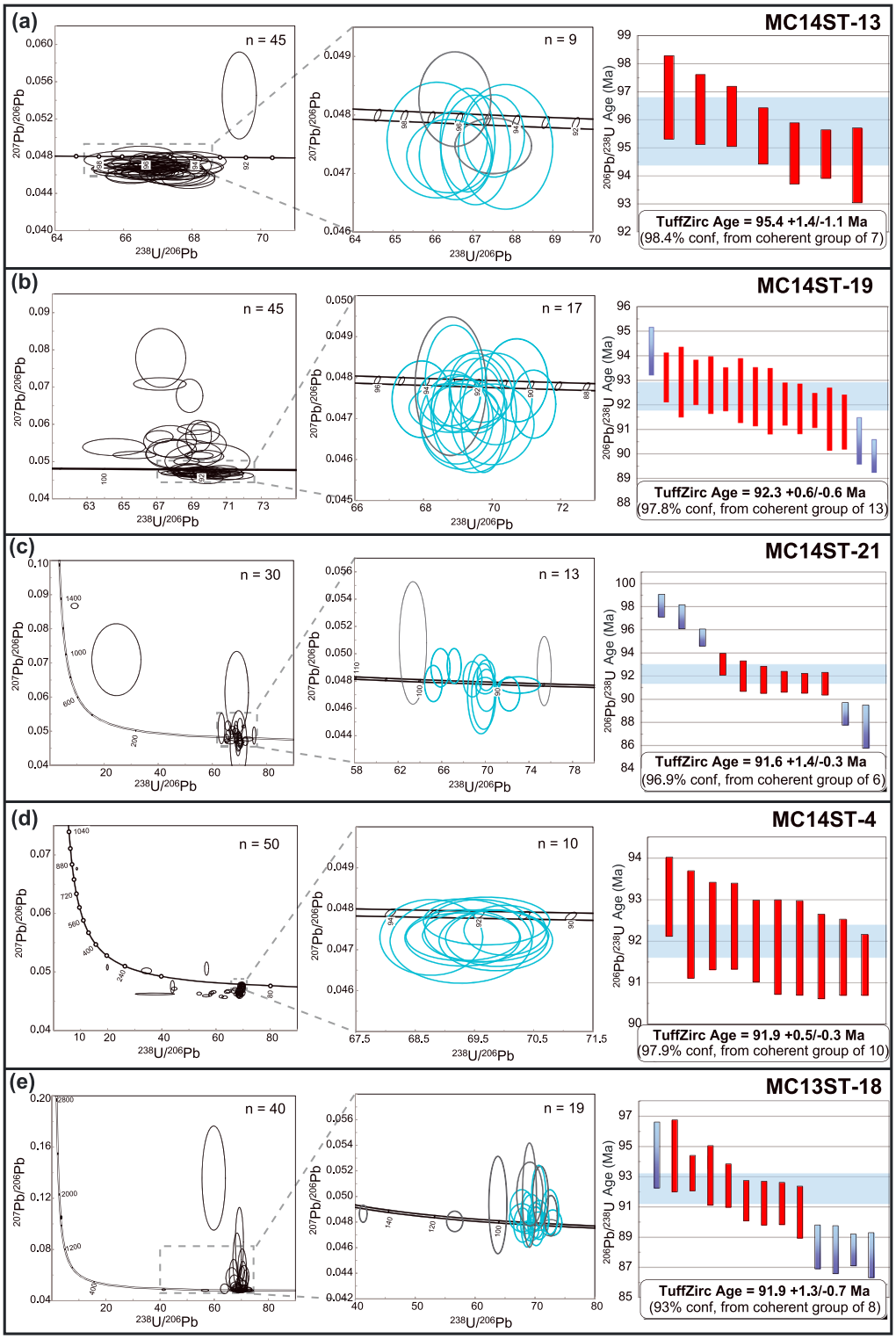

Figure 11. Zircon U-Pb data of magmatically foliated igneous rocks. For each sample, all of the analyses obtained are shown on a Tera-Wasserburg diagram to the left; those statistically concordant (i.e., overlapping the concordia line within error) data are plotted on a Tera-Wasserburg diagram in the middle; of the concordant analyses, those likely not affected by common Pb are plotted on a TuffZirc age diagram [*Ludwig*, 2012] to the right (highlighted with blue color on the Tera-Wasserburg diagram in the middle). On the TuffZirc age plot, red boxes are the error bars for the inferred syngenetic zircons; blue boxes are the error bars for the interpreted inherited zircons or those likely having experienced Pb loss; the horizontal blue band shows the inferred age and error of the syngenetic zircons. Multiple spot analyses on individual grain were all included in the results if they are different beyond two sigma errors; otherwise, only the analyses with lower discordance were used. All error ellipses and bars are shown at the 2σ level.

19449194, 2017, 3, Downloaded from https://agupubs.onlinelibrary.wiley.com/doi/10.1002/2016TC004264 by Auburn University Libraries, Wiley Online Library on [27/10/2022]. See the Terms and Conditions (https://onlinelibrary.wiley.com/terms-and-conditions) on Wiley Online Library for rules of use; OA articles are governed by the applicable Creative Commons License

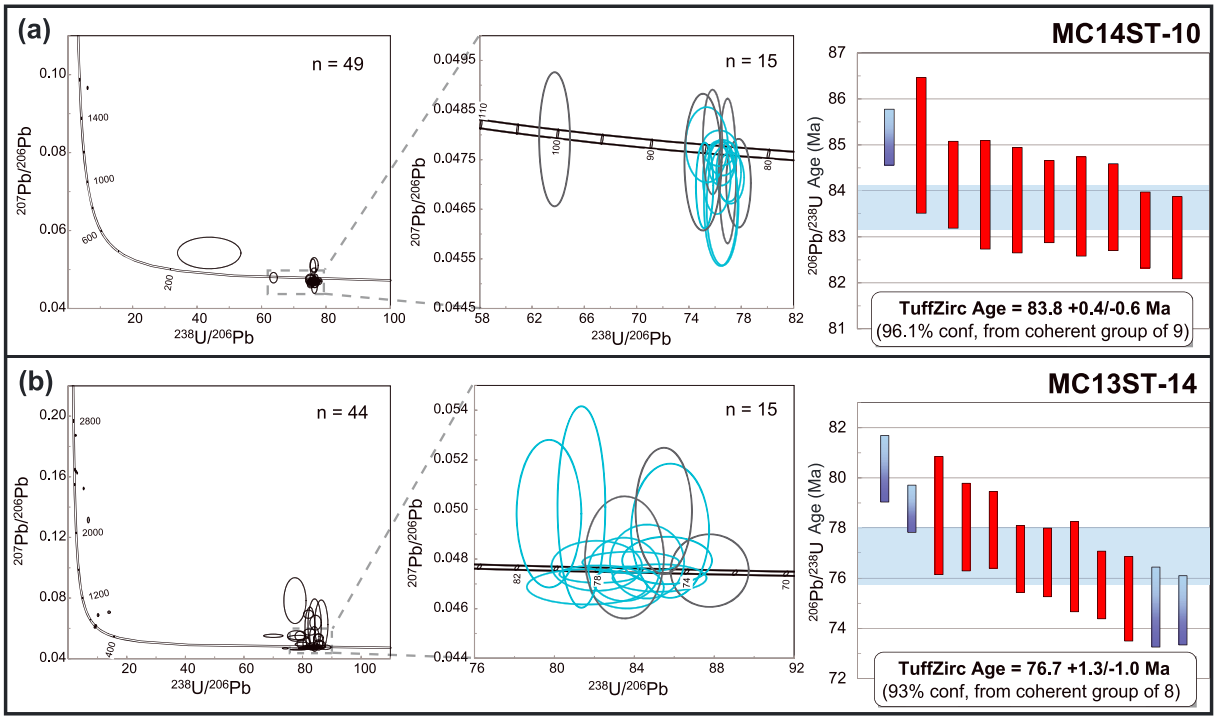

Figure 12. Zircon U-Pb data of unfoliated igneous rocks. See Figure 11 for plot descriptions.

crystallization. The interiors of a few zircons give Proterozoic ages (Figures 11c, 11d, 11e, and 12). Results from each sample are reported individually below.

4.2.1. Foliated Igneous Rocks

Sample MC14ST-13 was obtained from a tens of meter-scale, biotite-rich, coarse-grained granitic intrusion with magmatic foliations defined by biotite trails within quartzofeldspathic gneiss (Figure 6e). Quartz, feldspar, and biotite are not deformed at the microscale. Zircons from this sample are relatively large (100–300 μm). Nine out of 45 zircons yield concordant $^{206}Pb/^{238}U$ ages of ca. 94.4–96.8 Ma (Table S2), and seven of them give a TuffZirc age of 95.4 + 1.4/−1.1 Ma (Figure 11a).

Samples MC14ST-19 and MC14ST-21 were collected from foliated Idaho batholith granodiorite (Figure 6a) along the western edge of the SMC (Figure 2). These two samples are largely composed of coarse-grained, undeformed quartz, plagioclase, alkali feldspar, and biotite. They show a strong magmatic foliation at hand sample scale (Figure 6a) and weakly aligned euhedral minerals at the microscale. Zircons from these two samples range in size from 80 μm to 150 μm. Seventeen zircons from sample MC14ST-19 give concordant $^{206}Pb/^{238}U$ ages of ca. 89.9–94.2 Ma (Table S2), and 13 yield a TuffZirc age of 92.3 ± 0.6 Ma (Figure 11b). Thirteen zircons from sample MC14ST-21 give concordant $^{206}Pb/^{238}U$ ages of ca. 84.9–101.0 Ma (Table S2), and six yield a TuffZirc age of 91.6 + 1.4/−0.3 Ma (Figure 11c).

Sample MC14ST-4 was obtained from a 5–10 cm wide, coarse-grained felsic intrusive dike in biotite-rich quartzofeldspathic gneiss (Figure 6b). Undeformed quartz, feldspar, and biotite are weakly aligned as foliations at the microscale. The zircons analyzed range in size from 100 μm to 250 μm. Ten zircons from this sample yield concordant $^{206}Pb/^{238}U$ ages of ca. 91.4–93.1 Ma, and another zircon contains a core that gives a concordant $^{206}Pb/^{238}U$ age of 185.2 ± 8.3 Ma (2σ, Table S2). An inherited zircon core of 707.4 ± 17.9 Ma (2σ, 5.0% discordant, $^{207}Pb/^{235}U$ versus $^{206}Pb/^{238}U$) is also detected in this sample (Table S2). The 10 concordant zircons give a TuffZirc age of 91.9 + 0.5/−0.3 Ma (Figure 11d).

Sample MC13ST-18 was collected from a coarse-grained granitic dike (~0.5 m wide) that intruded a metagabbro body (Figure 6d). Euhedral quartz, alkali feldspar, and biotite form equigranular or porphyritic textures. The euhedral biotite is concentrated along layers defining the foliation of this intrusion. Zircons from this sample vary from 40 μm to 300 μm. Nineteen zircons yield concordant $^{206}Pb/^{238}U$ ages of ca. 87.8–154.2 Ma

19449194, 2017, 3, Downloaded from https://agupubs.onlinelibrary.wiley.com/doi/10.1002/2016TC004264 by Auburn University Libraries, Wiley Online Library on [27/10/2022]. See the Terms and Conditions (https://onlinelibrary.wiley.com/terms-and-conditions) on Wiley Online Library for rules of use; OA articles are governed by the applicable Creative Commons License

(Table S2). An inherited zircon core of 1617.0 ± 20.8 Ma (2σ, 8.8% discordant, $^{207}Pb/^{206}Pb$ versus $^{206}Pb/^{238}U$) is present in this sample (Table S2). Eight of the 19 concordant zircons give a TuffZirc age of 91.9 + 1.3/−0.7 Ma (Figure 11e).

4.2.2. Unfoliated Igneous Rocks

Leucogranite boudins are abundant in mica schist and are lozenge shaped on the horizontal surface (Figure 6f), indicating east-west flattening and north-south elongation. Sample MC14ST-10 was obtained from a boudinaged leucogranite dike (~25 cm wide) within the mica schist. It shows no foliation and consists of undeformed, medium-grained quartz, feldspar, and white mica. Zircons analyzed from this sample range from 100 μm to 250 μm. Fourteen zircons yield concordant $^{206}Pb/^{238}U$ ages of ca. 82.3–85.3 Ma, and another grain gives a concordant $^{206}Pb/^{238}U$ age of 100.4 ± 1.5 Ma (2σ, Table S2). Nine of these concordant zircons yield a TuffZirc age of 83.8 + 0.4/−0.6 Ma (Figure 12a).

Sample MC13ST-14 was collected from an undeformed intrusion of pegmatitic biotite leucogranite within metapsammite. Biotite grains are up to ~2 cm long and are randomly distributed among quartz and feldspar (Figure 6g), indicating absence of deformation. Zircons analyzed from this sample range in size from 100 μm to 200 μm. Fifteen grains yield concordant $^{206}Pb/^{238}U$ ages of ca. 73.0–80.4 Ma (Table S2). Four inherited grains give $^{206}Pb/^{238}U$ ages of 603.6 ± 11.6 Ma, 653.0 ± 17.1 Ma, and 668.9 ± 16.5 Ma, and a $^{207}Pb/^{206}Pb$ age of 2559.0 ± 8.0 Ma (Table S2). Eight of the 15 Cretaceous zircons give a TuffZirc age of 76.7 + 1.3/−1.0 Ma (Figure 12b).

5. Discussion

5.1. Transpressional Strain Partitioning into Wrench (Shear)- and Contraction-Dominated Domains

A typical transpressional shear zone is characterized by three-dimensional deformation simultaneously combining horizontal strike-slip shearing, orthogonal shortening across, and vertical lengthening along the shear plane [*Sanderson and Marchini*, 1984]. The SMC deformational fabrics and structures contain evidence for the three components of a transpressional zone in which the strike-slip shearing is the most prominent component.

The predominant strike-slip shearing component is mainly recorded in the SMC wrench-dominated domains represented by the subvertical mylonitic foliation striking roughly north-south and the subhorizontal mineral lineation that plunges shallowly to the north or south (Figures 3a and 3b, stereoplots i–iii). The degree of shearing is high, which is reflected by developments of the pervasive winged porphyroclasts/blocks and S-C structures at mesoscale and microscale, as well as the remarkable mineral stretching lineations (Figure 4). Sheath folds with various hinge-line curvatures ranging from >90° to >160° (Figures 5c and 5d) along the shear plane also suggest a progressive and high-degree shearing component [*Alsop and Holdsworth*, 2006]. These sheath folds are interpreted to have formed during shearing on the basis of evidence that the fold axis and axial plane of the sheath folds are parallel to the lineation and foliation of the shear zones [*Carreras et al.,* 2005].

The horizontal, approximately east-west shortening component orthogonal to the strike-slip component is largely preserved in the contraction-dominated domains represented by roughly north-south-trending folds (Figures 8a and 8b) and thrusts (Figures 8d and 8e). Of the two kinds of lineations on the folded surfaces, i.e., north-south-trending, subhorizontal- to shallow-plunging mineral lineations (strike-slip) (Figure 3c, stereoplots i–iii) and east-west- to NE-SW-trending, shallow- to subvertical-plunging slip lineations (dip-slip) (Figure 3c, stereoplot i), the strike-slip lineations are predominant whereas the dip-slip lineations are only preserved locally with folds. This suggests that the horizontal shortening component was not large enough to trigger switching of the stretching lineation from horizontal to vertical as proposed may happen for a wrench-dominated transpressional zone [*Fossen and Tikoff*, 1993; *Tikoff and Teyssier*, 1994; *Tikoff and Greene*, 1997]. The curvilinear form of the SMC folds indicated by the variable fold hinge plunges (Figure 3c, stereoplots i–iii) suggests that the folds were rotated around the pole to axial plane during the transpressional deformation.

The vertical lengthening component is primarily documented in the contraction-dominated domains by folds and thrusts as a result of the pure shear component of transpression. Development of steep dip-slip lineations (Figures 8c and 3c, stereoplot i) orthogonal to the strike-slip lineations additionally indicates the

19449194, 2017, 3, Downloaded from https://agupubs.onlinelibrary.wiley.com/doi/10.1002/2016TC004264 by Auburn University Libraries, Wiley Online Library on [27/10/2022]. See the Terms and Conditions (https://onlinelibrary.wiley.com/terms-and-conditions) on Wiley Online Library for rules of use; OA articles are governed by the applicable Creative Commons License

existence of vertical lengthening. The vertical lengthening component is also reflected in the wrench-dominated domains. For example, centimeter-scale isoclinal folds (Figures 9a and 9b) in wrench-dominated domains contain fold axes and axial planes parallel to the lineation and foliation of the shear zone. Regardless of whether they are preexisting folds that have been transposed during shearing or completely formed during shearing, formation of these isoclinal folds in a shear zone interior indicates occurrences of vertical lengthening along (see the arrows in Figures 9a and 9b) and horizontal shortening across the shear plane. Moreover, the S-C structures that are composed of boudinaged quartzofeldspathic blocks (Figures 9c and 9d) in the cross-sectional view also suggest vertical lengthening along the shear plane. The east-up-and-west-down (Figure 9c) and west-up-and-east-down (Figure 9d) vertical movements revealed by those S-C structures that are parallel to each other indicate that the vertical lengthening component had a two-direction movement, i.e., up and down. The upward and downward transportation might have happened concurrently or one after another during the deformation.

These components of transpressional deformation are considered to be broadly coeval on the basis of the mutually crosscutting relationships (Figure 10) and the general compatible structures and fabrics, although another early phase of shortening cannot be ruled out. The contractional components (horizontal shortening plus vertical lengthening) are relatively small because of the absence of dip-slip lineation in wrench-dominated domains and the rare occurrence of dip-slip lineation in the contraction-dominated domains. Hence, with the domainal subhorizontal strike-slip lineations across the area studied, the SMC is consistent with a wrench-dominated transpressional zone [*Tikoff and Greene*, 1997]. In the SMC transpressional zone, the maximum stretching direction (the strike-slip component) is approximately north-south and the minimum stretching direction (the shortening component) is about east-west, both of which are about horizontal whereas the intermediate stretching direction (the lengthening component) is roughly vertical.

Generally, fabric orientation in a transpression zone is principally controlled by the angle of obliquity, intensity of finite strain, and degree of kinematic partitioning [e.g., *Fossen and Tikoff*, 1993; *Tikoff and Teyssier*, 1994; *Teyssier et al.,* 1995; *Tikoff and Greene*, 1997; *Dewey et al.,* 1998]. The SMC structural fabrics show several key characters as a transpressionally deformed zone: (1) Subhorizontal lineations developed in both the wrench- and contraction-dominated domains suggest that either the angle of convergence is low (<5–10°) or the deformation has a relatively low finite strain [*Tikoff and Greene*, 1997] with an angle of convergence less than 20° as required for a wrench-dominated transpressional zone [*Fossen and Tikoff*, 1993; *Tikoff and Teyssier*, 1994; *Teyssier et al.,* 1995]. (2) There might be volume change during the deformation, because similar folds (i.e., flow folds) occur on the movement plane along shear zones and they are an indicator of mass transport and volume change [*Passchier*, 2001]. (3) Subparallelism of folds and thrusts with shear zones suggests that the folds and thrusts might have initiated at much lower angles than 45° relative to the shear zones [*Sanderson and Marchini*, 1984] or that the simple shear component of the transpressional deformation might have accommodated large amounts of displacement [*Fossen and Tikoff*, 1998]. The SMC transpressional deformation is viewed as a zone of discontinuous partitioning of strain [e.g., *Dewey et al.,* 1998] into wrench- and contraction-dominated domains across strike (Figure 13).

5.2. Magma-Facilitated Partitioning of Deformation

The discontinuous nature of the SMC transpressional deformation was facilitated by emplacement of felsic intrusive sheets within the metasedimentary rocks (Figure 13) and variations in lithology of the host rocks. For most of the intrusive sheets (e.g., Figures 6a–6e), euhedral biotite and feldspar that are aligned along layers defining magmatic foliations suggest that the intrusive sheets were still ductile during the process of deformation that induces flow of the melt rather than exerts strain on individual minerals within the melt. This texture is expected when melts are emplaced during regional deformation [e.g., *Paterson et al.,* 1989]. The parallelism between the intrusive contacts, magmatic foliation of the intrusive sheets, and the mylonitic fabrics of the surrounding metasedimentary rocks (Figures 3a and 3b, stereoplots i–iii) is consistent with the synchronous feature of magma emplacement and the transpressional deformation in the SMC. The felsic magmas,therefore most likely accommodated a fraction of the deformation. As magmatism tends to localize shear in a transpressional zone [e.g., *Saint Blanquat et al.,* 1998; *Brown and Solar*, 1998] and the partially melted zone remains weak during shearing, the strike-slip motion would be efficiently facilitated by syntectonic emplacement of intrusions.

19449194, 2017, 3, Downloaded from https://agupubs.onlinelibrary.wiley.com/doi/10.1002/2016TC004264 by Auburn University Libraries, Wiley Online Library on [27/10/2022]. See the Terms and Conditions (https://onlinelibrary.wiley.com/terms-and-conditions) on Wiley Online Library for rules of use; OA articles are governed by the applicable Creative Commons License

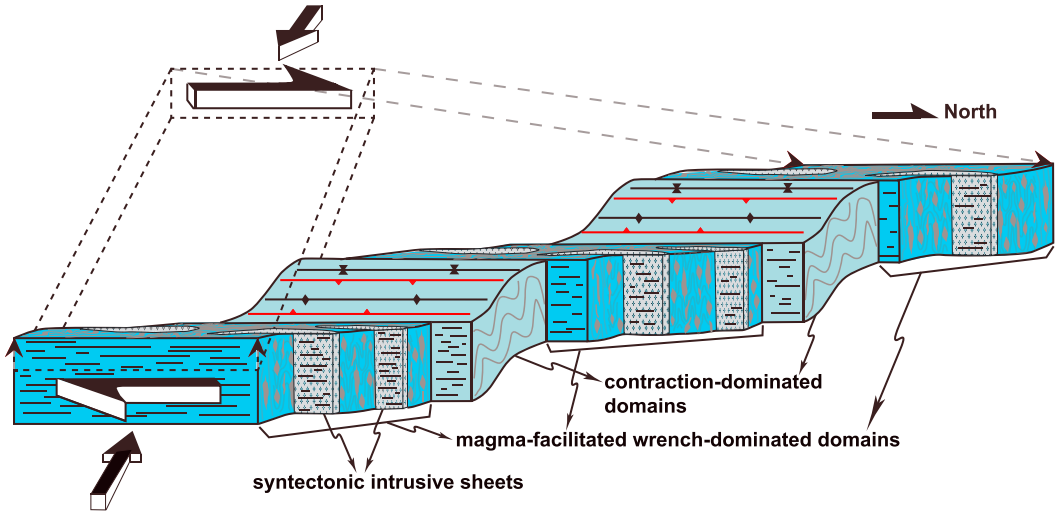

Figure 13. A schematic three-dimensional diagram showing the Sawtooth metamorphic complex transpressional zone consisting of magma-facilitated wrench (shear)-dominated domains and contraction-dominated domains. Dashed shape represents the original position and thickness of the undeformed block. Lines (red) with single triangles indicate thrust faults, and lines (black) with paired triangles denote folds. Horizontal lineations are shown in shear planes; folds and sheared blocks are shown in cross sections.

Deformation of the SMC intrusive sheets therefore may have accommodated more strike-slip displacements than that of the surrounding metasedimentary rocks, because rheological contrast between magmas and their country rocks facilitates strain partitioning [*Vigneresse and Tikoff*, 1999]. This premise is supported by the development of strong S-C structures and pervasive winged porphyroclasts in the intrusive sheets (e.g., Figures 6a–6e). The SMC transpressional partitioning therefore is more discontinuous across the magmatically foliated intrusive sheets.

Feedback relations exist between emplacement of melts and formation of shear zones in orogenic belts [*Brown and Solar,* 1998]. In the SMC, the magmatically foliated intrusive sheets predominantly occur in the wrench-dominated domains, perhaps because strike-slip shear zones provide a higher-pressure gradient along the vertical orientation and preferential pathways for rising magmas aided by buoyancy-induced overpressures [*Saint Blanquat et al.,* 1998; *Brown and Solar*, 1998]. The emplacements of the magmatically foliated magmas might also have thermally weakened the vertical shear zones to facilitate the strike-slip partitioning of the transpressional deformation [e.g., *Saint Blanquat et al.,* 1998].

Bulk-rock compositions also have an impact on localizing shear zones in the SMC. The rheologically weak units such as mica schist, marble, calc-silicate gneiss, and biotite-rich quartzofeldspathic gneiss generally contain stronger shear fabrics than those in quartzofeldspathic gneiss and metapsammite, which suggests that the abundant mica and calcite that are more easily deformed played an important role on localizing strain. This along with the lines of evidence stated above suggests that the partitioning of strain was largely controlled by the bulk rheology of the SMC metasedimentary rocks and the distribution of fluids/melts within them.

5.3. Timing of Deformation

The parallelism of the magmatic foliations of the felsic intrusive sheets and the solid-state mylonitic fabrics of the metasedimentary rocks across the study area indicates that the emplacements of the intrusive sheets and the SMC transpressional deformation were broadly coeval. Thus, the crystallization ages of zircons from the intrusive sheets defines the timing of deformation.

Samples MC14ST-21 (Figure 6a), MC14ST-19 (Figure 6a), MC14ST-4 (Figure 6b), MC13ST-18 (Figure 6d), and MC14ST-13 (Figure 6e) (see Figure 2 for locations) are characterized by syntectonic magmatic foliations. Magmatic zircons from these five samples give crystallization ages ranging between ca. 95 and ca. 92 Ma (Figure 11). The period of ca. 95–92 Ma therefore likely represents the timing of the main phase deformation in the SMC transpressional zone.

19449194, 2017, 3, Downloaded from https://agupubs.onlinelibrary.wiley.com/doi/10.1002/2016TC004264 by Auburn University Libraries, Wiley Online Library on [27/10/2022]. See the Terms and Conditions (https://onlinelibrary.wiley.com/terms-and-conditions) on Wiley Online Library for rules of use; OA articles are governed by the applicable Creative Commons License

19449194, 2017, 3, Downloaded from https://agupubs.onlinelibrary.wiley.com/doi/10.1002/2016TC004264 by Auburn University Libraries, Wiley Online Library on [27/10/2022]. See the Terms and Conditions (https://onlinelibrary.wiley.com/terms-and-conditions) on Wiley Online Library for rules of use; OA articles are governed by the applicable Creative Commons License

Sample MC14ST-10 (Figure 6f) lacks magmatic foliation but is boudinaged into lozenge shapes, which indicates that this sample has undergone a less ductile deformation characterized by east-west contraction. It is therefore interpreted as a strain marker of the late-stage deformation in the SMC transpressional zone. Magmatic zircons from this sample give an age of ca. 84 Ma (Figure 12a).

Sample MC13ST-14 (Figure 6g) is pegmatitic, showing no hint of deformation, and therefore constrains the timing of the final deformation in the SMC transpressional zone. The magmatic zircons analyzed from this sample indicate that the SMC deformation ceased by ca. 77 Ma (Figure 12b).

Based on the syntectonic intrusions, the SMC transpressional deformation was most intense at ca. 95–92 Ma, may have remained active with less strain through ca. 84 Ma, and had ended by ca. 77 Ma. These data do not preclude deformation prior to the emplacements of the magmatically foliated intrusive sheets. Further, the exact division of the main phase and late-stage of deformation is uncertain but likely to be between ca. 92 and 84 Ma. Based on the crystallization ages and the location of these intrusions within the Idaho batholith, the magmatically foliated intrusive sheets in the SMC may be associated with the early metaluminous and border zone plutons (~100–85 Ma) in the Atlanta lobe of the Idaho batholith [*Gaschnig et al.,* 2010].

The timing of deformation revealed by the magmatically foliated intrusive sheets is consistent with the ages of metamorphic or hydrothermal overgrowths of detrital zircons from the SMC metapsammites. The metapsammites from highly sheared units often contain abundant zircon with Archean to early Paleozoic detrital cores and wide ($>30\,\mu m$) overgrowths that give Cretaceous ages of ca. 92–89 Ma [*Bergeron*, 2012; *Ma et al.,* 2016]. The consistence of age between the detrital zircon overgrowths and magmatic zircons from the magmatically foliated intrusive sheets, along with the compatible fabrics between the metapsammites and those other metasedimentary/intrusive rocks, suggests that the metamorphic or hydrothermal overgrowths on detrital zircons are contemporaneous with and probably genetically related to the SMC transpressional deformation.

5.4. Contribution to Orogen-Parallel Translations in the Northern U.S. Cordillera

In the northern U.S. Cordillera, the WISZ is a major north-south striking structure that is inferred to have accommodated orogen-parallel translation of outboard terranes [*Oldow et al.,* 1989; *Saleeby and Busby-Spera*, 1992; *Dickinson*, 2004, 2006; *Gray and Oldow*, 2005; *Wyld et al.,* 2006]. The WISZ is interpreted as a contraction-dominated transpressional zone [*Manduca et al.,* 1993; *McClelland et al.,* 2000] with the main phase of deformation during ca. 105–90 Ma [*Giorgis et al.,* 2008]. It is suggested that the WISZ has accommodated a limited amount of dextral strike-slip movement [*Giorgis et al.,* 2005], perhaps as small as ~50 km [*Giorgis and Tikoff*, 2004]. Other studies, however, suggest that there are large amounts of displacement up to several hundred kilometers associated with translation of the Blue Mountains [e.g., *Wyld and Wright*, 2001; *Housen and Dorsey*, 2005; *Wright and Wyld*, 2007]. A ~400 km-scale northward translation of the Blue Mountains along the WISZ is supported by the detrital zircon study of *LaMaskin et al.* [2011]. Therefore, there is a discrepancy between the amount of dextral simple shear strain recorded in the WISZ and the amount of dextral strike-slip translation required after docking of the Blue Mountains terranes. Additional dextral strike-slip translation may have been accommodated by other coeval and/or subsequent shear zones subparallel to the WISZ. It has been suggested that the strike-slip shearing may have continued after the main WISZ deformation on structures east of the WISZ in the Idaho batholith [e.g., *Fleck and Criss*, 2004; *Giorgis et al.,* 2008].

Orogen-parallel translation in orogenic belts is commonly accommodated by many anastomosing strike-slip faults in an oblique convergent setting [e.g., *Umhoefer*, 2000; *Foster et al.,* 2009]. Dextral transpressional deformation in the SMC is subparallel with that of the WISZ, and their timing of deformation is consistent, which suggests that these two shear zones form a single shear system. The major difference between the two shear zones is the relative magnitudes of the simple shear and pure shear components of transpression; the SMC has a subhorizontal lineation indicative of a simple-shear-dominated transpression whereas the WISZ has a subvertical lineation that indicates a pure-shear-dominated transpression. This difference might be due to their locations relative to the suture zone or the younger age of the main phase of deformation in the SMC than that in the WISZ.

Zircon U-Pb geochronology of syntectonic intrusive sheets indicates that the main phase of deformation in the SMC transpressional zone is between ca. 95 Ma and ca. 92 Ma. The main SMC deformation therefore

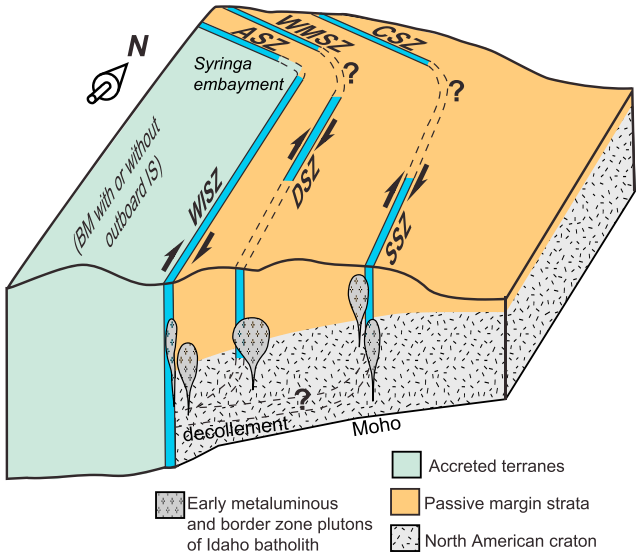

Figure 14. A three-dimensional sketch showing the regional transpression system including the Western Idaho shear zone (WISZ), Deadwood shear zone (DSZ), and Sawtooth shear zone (SSZ), along with their connections to the north, Ahsahka shear zone (ASZ), Woodrat Mountain shear zone (WMSZ), and Clearwater shear zone (CSZ), respectively. Note that width of shear zones is not to scale. Early metaluminous and border zone plutons of the Idaho batholith are after that of *Gaschnig et al.* [2010]. BM = Blue Mountains province, IS = Insular Superterrane.

was contemporaneous with the main WISZ deformation at least between ca. 95 and ca. 92 Ma. The timing of the late-stage deformation (~84 Ma) in the SMC is also consistent with that of the WISZ. Zircons from syntectonic tonalite in the WISZ give $^{206}Pb/^{238}U$ ages of ca. 90 Ma, and hornblende and biotite from samples of orthogneiss within the WISZ yield $^{40}Ar/^{39}Ar$ ages of ca. 80 Ma, which suggests that the late-stage deformation of the WISZ occurred between ca. 90 and ca. 80 Ma [*Giorgis et al.,* 2008].

The Deadwood shear zone (Figure 1a) is a ~2 km wide, 010°-trending deformation zone about 50 km east of the WISZ within the Idaho batholith [*Lund et al.,* 1997; *Lund*, 2004; *Montz et al*., 2013]. In this shear zone, granitic rocks and metasedimentary units show steeply dipping foliation and/or mylonitic fabrics recording a dextral movement [*Lund et al.,* 1997; *Lund*, 2004]. The deformed granites yield 83–86 Ma magmatic zircons and zircons of Neoproterozoic-Ordovician aged cores with 79–82 Ma rims [*Montz et al*., 2013]. This shear zone might be wider than currently documented, because anisotropy of magnetic susceptibility analyses indicates parallel fabrics in the adjacent Idaho batholith granites [*Montz et al*., 2013]. Therefore, similar to the Sawtooth shear zone, the Deadwood shear zone also has a dextral sense of shearing component and was possibly active during the late-stage of the WISZ deformation.

It is likely that a system of subparallel dextral strike-slip shear zones, including the WISZ, Sawtooth shear zone, and possibly the Deadwood shear zone, were active in the Idaho batholith region (Figure 14) during the Late Cretaceous, which have contributed jointly to the orogen-parallel translation of the outboard accreted terranes. These shear zones may or may not have been active at exactly the same time. Kinematic coupling of discrete crustal shear zones might be explained by movement of the strong lithospheric mantle underneath [*Saint Blanquat et al.,* 1998] or a common decollement system at the lower crust or upper mantle levels [*Oldow et al.,* 1990]. Considering the extensive thin- and thick-skinned deformation linked by basal decollements in this part of the North American Cordillera [*McClelland and Oldow,* 2004], the decollement model might be more appropriate (Figure 14). The depth of this decollement in south-central Idaho is estimated to have been about 55 km [*McClelland and Oldow,* 2004].

The existence of a regional transpressional system composed of multiple linked shear zones has important implications to the tectonic evolution of the Syringa embayment to the north (Figure 1a). The continuation of the WISZ into the Syringa embayment is unclear because of potential connections/interactions among multiple fault zones of various orientations. *McClelland and Oldow* [2004, 2007] suggest that the north-south WISZ is truncated by the northwest-striking Orofino shear zone containing the Ahsahka, Woodrat Mountain, and Clearwater shear zones (Figure 1a), whereas *Schmidt et al.* [2016] propose that the WISZ continues to the north into the northwest-striking Ahsahka shear zone although it is displaced by a northeast-striking local fault, the Mt Idaho zone (Figure 1a). The main evidence for the truncation of the WISZ by the Orofino shear zone is that the northeast portion of the latter, i.e., the Clearwater shear zone, extends to the east of the WISZ [*McClelland and Oldow,* 2007]. The present study documents a kinematically compatible transpressive shear zone well east of the WISZ in the Sawtooth metamorphic complex, which opens a possibility that the displacement of the Sawtooth shear zone continues to the north into the Clearwater shear zone (Figure 14).

19449194, 2017, 3, Downloaded from https://agupubs.onlinelibrary.wiley.com/doi/10.1002/2016TC004264 by Auburn University Libraries, Wiley Online Library on [27/10/2022]. See the Terms and Conditions (https://onlinelibrary.wiley.com/terms-and-conditions) on Wiley Online Library for rules of use; OA articles are governed by the applicable Creative Commons License

19449194, 2017, 3, Downloaded from https://agupubs.onlinelibrary.wiley.com/doi/10.1002/2016TC004264 by Auburn University Libraries, Wiley Online Library on [27/10/2022]. See the Terms and Conditions (https://onlinelibrary.wiley.com/terms-and-conditions) on Wiley Online Library for rules of use; OA articles are governed by the applicable Creative Commons License

Similarly, the Deadwood shear zone could be linked to the Woodrat Mountain shear zone, and the WISZ might be originally connected with the Ahsahka shear zone (Figure 14). These interpretations are supported by lines of evidence from two aspects: compatible kinematics and timing. The subparallel Ahsahka, Woodrat Mountain, and Clearwater shear zones have a common kinematics (reverse, top-to-the-southwest transpressive shearing) [*Schmidt et al.,* 2016] and seem to be deformed diachronously. The timing of the Ahsahka shear zone is constrained to be ca. 116–92 Ma (main phase deformation) through ca. 87 Ma (late-stage deformation) to ca. 80 Ma [*Schmidt et al.,* 2016]. The Clearwater shear zone is known to be active at least during ca. 94–73 Ma [*McClelland and Oldow,* 2007*; Lund et al.,* 2008]. The timing of the Woodrat Mountain shear zone is less well constrained, but it might be initiated prior to the deformation of the Ahsahka shear zone on the basis of relative fabrics and structural relationships [*Schmidt et al.,* 2016]. The deformation of these three shear zones therefore was broadly coeval with that of the WISZ, Deadwood, and Sawtooth shear zones. Moreover, the top-to-the-southwest transpressive shearing of those northwest-striking shear zones to the north (ASZ, WMSZ, and CSZ of Figure 14) and the dextrally strike-slip transpressive shearing of those north-south shear zones to the south (WISZ, DSZ, and SSZ of Figure 14) are kinematically consistent with the northeast-directed convergence along the curved margin of the North American craton proposed by *Giorgis et al.* [2016]. A larger system of linked contemporaneous shear zones is therefore well supported by the existing data from each zone and suggests that northward transport of accreted terranes was accommodated on numerous orogen-parallel structures.

6. Conclusions

The SMC contains the three deformational components of a transpressional zone, i.e., strike-slip shearing, orthogonal shortening, and vertical lengthening. These components are partitioned into wrench (shear)- and contraction-dominated domains, and they were broadly coeval based on mutually crosscutting relationships and general compatible structures and fabrics. The partitioning of deformation was facilitated by emplacement of magmatically foliated intrusive sheets in the shear-dominated domains. The fabrics of the SMC are consistent with that of a wrench-dominated transpressional zone.

U-Pb dating of magmatic zircons from syntectonic, magmatically foliated intrusive sheets reveals that the SMC transpressional zone experienced intense deformation in ca. 95–92 Ma, underwent late-stage deformation through ca. 84 Ma, and ceased movement by ca. 77 Ma.

The SMC transpressional zone is kinematically compatible with the WISZ and was developed contemporaneously with some of the deformation in the WISZ. The SMC and the WISZ may belong to a single regional transpression system, and they have likely contributed together to the northward orogen-parallel translation of accreted terranes by accommodating dextral strike-slip shearing during the Late Cretaceous.

Acknowledgments

Scott Giorgis, Bill McClelland, and the Associate Editor, John Geissman, are thanked for their helpful comments and suggestions. This research was supported by the National Science Foundation grants EAR-1145212 to Mueller and Foster and EAR-1145073 to Dutrow. We thank the Colorado Scientific Society and the Geological Society of America for partial financial support of Ma's fieldwork. Suite Xu and Chrissy Allen are deeply thanked for field assistance. We are grateful to David Fluetsch and Lieze Dean of the National Forest Service for permitting sample collection within the Sawtooth National Recreation Area. Ann Heatherington and George Kamenov are acknowledged for assistance with the zircon analyses. The sample locations and zircon U-Pb data presented in this study are provided in the supporting information. Foliation and lineation data are available from the corresponding author on request (macmachong@gmail.com).

References

Alsop, G., and R. Holdsworth (2006), Sheath folds as discriminators of bulk strain type, *J. Struct. Geol.*, *28*, 1588–1606.

Bergeron, P. G. (2012), U-Pb Geochronology of detrital zircon in quartzites of the Sawtooth metamorphic complex, Sawtooth Range, Idaho, U.S.A, MS thesis, 174 pp., Louisiana State Univ., Baton Rouge, La. [Available at http://etd.lsu.edu/docs/available/etd-11142012-113110/.]

Black, L. P., S. L. Kamo, I. S. Williams, R. Mundil, D. W. Davis, R. J. Korsch, and C. Foudoulis (2003), The application of SHRIMP to Phanerozoic geochronology; a critical appraisal of four zircon standards, *Chem. Geol.*, *200*, 171–188.

Black, L. P., S. L. Kamo, C. M. Allen, D. W. Davis, J. N. Aleinikoff, J. W. Valley, R. Mundil, I. H. Campbell, R. J. Korsch, and I. S. Williams (2004), Improved $^{206}Pb/^{238}U$ microprobe geochronology by the monitoring of a trace-element-related matrix effect; SHRIMP, ID-TIMS, ELA-ICP-MS and oxygen isotope documentation for a series of zircon standards, *Chem. Geol.*, *205*, 115–140.

Blake, D. E., K. D. Gray, S. Giorgis, and B. Tikoff (2009), A tectonic transect through the Salmon River suture zone along the Salmon River Canyon in the Riggins region of west-central Idaho, in *Volcanoes to Vineyards: Geologic Field Trips through the Dynamic Landscape of the Pacific Northwest*, *Geological Society of America Field Guide*, vol. 15, edited by J. E. O'Connor, R. J. Dorsey, and I. P. Madin, pp. 345–372.

Brown, M., and G. S. Solar (1998), Shear-zone systems and melts: Feedback relations and self-organization in orogenic belts, *J. Struct. Geol.*, *20*, 211–227.

Burchfiel, B., D. Cowan, and G. Davis (1992), Tectonic overview of the Cordilleran orogen in the western United States, in *The Cordilleran Orogen: Conterminous U.S*, vol. G3, edited by B. Burchfiel, P. Lipman, and M. Zoback, pp. 407–479, Geol. Soc. Am., Boulder, Colo.

Carreras, J., E. Druguet, and A. Griera (2005), Shear zone-related folds, *J. Struct. Geol.*, *27*, 1229–1251.

Davis, J. R., and S. Giorgis (2014), An inverse approach to constraining strain and vorticity using rigid clast shape preferred orientation data, *J. Struct. Geol.*, *68*, 337–346.

Dewey, J., R. Holdsworth, and R. Strachan (1998), *Transpression and Transtension Zones*, *Geol. Soc. London, Spec. Publ.*, vol. 135, pp. 1–14.

Dickinson, W. R. (2004), Evolution of the North American Cordillera, *Annu. Rev. Earth Planet. Sci.*, *32*, 13–45.

Dickinson, W. R. (2006), Geotectonic evolution of the Great Basin, *Geosphere*, *2*, 353–368.

Dorsey, R. J., and T. A. LaMaskin (2007), Stratigraphic record of Triassic-Jurassic collisional tectonics in the Blue Mountains province, northeastern Oregon, *Am. J. Sci.*, *307*, 1167–1193.

Dutrow, B., S. Anderson, D. Henry, and P. Mueller (1995), A new Precambrian crustal province in south-central Idaho?, *Eos Trans. AGU*, *76*, 678.
Dutrow, B., D. Henry, I. Fukai, and P. Mueller (2014), Metamorphism in the Sawtooth metamorphic complex, Idaho: Constraints on the middle crust, Geological Society of America Abstracts with Programs, vol. 46, 96 pp.
Fisher, F. S., D. H. McIntyre, and K. M. Johnson (1992), Geologic map of the Challis 1° × 2° quadrangle, Idaho, U.S. Geol. Surv. Miscellaneous Investigation Ser. Map I-1819, scale 1:250,000. [Available at http://pubs.usgs.gov/imap/i-1819.]
Fleck, R. J., and R. Criss (2004), Location, age and tectonic significance of the western Idaho suture zone (WISZ), 48 pp., U.S. Geol. Surv. Open-File Report 2004-1039. [Available at http://pubs.usgs.gov/of/2004/1039.]
Fossen, H., and B. Tikoff (1993), The deformation matrix for simultaneous simple shearing, pure shearing and volume change, and its application to transpression-transtension tectonics, *J. Struct. Geol.*, *15*, 413–422.
Fossen, H., and B. Tikoff (1998), Extended models of transpression and transtension, and application to tectonic settings, in *Continental Transpressional and Transtensional Tectonics*, *Geol. Soc. London, Spec. Publ.*, vol. 135, edited by R. E. Holdsworth, R. A. Strachan, and J. F. Dewey, pp. 15–33.
Foster, D. A., B. D. Goscombe, and D. R. Gray (2009), Rapid exhumation of deep crust in an obliquely convergent orogen: The Kaoko Belt of the Damara Orogen, *Tectonics*, *28*, TC4002, doi:10.1029/2008TC002317.
Fukai, I. (2013), Metamorphic and geochemical signatures of calc-silicate gneisses from the Sawtooth metamorphic complex, Idaho, U.S.A.: Implications for crustal evolution in western North America, MS thesis, 202 pp., Louisiana State Univ., Baton Rouge, La. [Available at http://etd.lsu.edu/docs/available/etd-04122013-180236/.]
Gaschnig, R. M., J. D. Vervoort, R. S. Lewis, and W. C. McClelland (2010), Migrating magmatism in the northern US Cordillera: In situ U–Pb geochronology of the Idaho batholith, *Contrib. Mineral. Petrol.*, *159*, 863–883.
Getty, S. R., J. Selverstone, B. P. Wernicke, S. B. Jacobsen, E. Aliberti, and D. R. Lux (1993), Sm-Nd dating of multiple garnet growth events in an arc-continent collision zone, northwestern U.S. Cordillera, *Contrib. Mineral. Petrol.*, *115*, 45–57.
Giorgis, S., and B. Tikoff (2004), *Constraints on Kinematics and Strain from Feldspar Porphyroclast Populations*, *Geol. Soc. London, Spec. Publ.*, vol. 224, pp. 265–286.
Giorgis, S., B. Tikoff, and W. McClelland (2005), Missing Idaho arc: Transpressional modification of the $^{87}Sr/^{86}Sr$ transition on the western edge of the Idaho batholith, *Geology*, *33*, 469–472.
Giorgis, S., W. McClelland, A. Fayon, B. S. Singer, and B. Tikoff (2008), Timing of deformation and exhumation in the western Idaho shear zone, McCall, Idaho, *Geol. Soc. Am. Bull.*, *120*, 1119–1133.
Giorgis, S., Z. Michels, L. Dair, N. Braudy, and B. Tikoff (2016), Kinematic and vorticity analyses of the western Idaho shear zone, USA, *Lithosphere*, doi:10.1130/l518.1.
Gray, K. D., and J. S. Oldow (2005), Contrasting structural histories of the Salmon River belt and Wallowa terrane: Implications for terrane accretion in northeastern Oregon and west-central Idaho, *Geol. Soc. Am. Bull.*, *117*, 687–706.
Housen, B. A., and R. J. Dorsey (2005), Paleomagnetism and tectonic significance of Albian and Cenomanian turbidites, Ochoco basin, Mitchell Inlier, central Oregon, *J. Geophys. Res.*, *110*, B07102, doi:10.1029/2004JB003458.
LaMaskin, T. A., J. D. Vervoort, R. J. Dorsey, and J. E. Wright (2011), Early Mesozoic paleogeography and tectonic evolution of the western United States: Insights from detrital zircon U-Pb geochronology, Blue Mountains Province, northeastern Oregon, *Geol. Soc. Am. Bull.*, *123*, 1939–1965.
LaMaskin, T. A., R. J. Dorsey, J. D. Vervoort, M. D. Schmitz, K. P. Tumpane, and N. O. Moore (2015), Westward growth of Laurentia by pre–Late Jurassic terrane accretion, eastern Oregon and western Idaho, United States, *J. Geol.*, *123*, 233–267.
Ludwig, K. R. (2012), User's manual for Isoplot 3.75: A geochronological toolkit for Microsoft Excel, 75 pp., Berkeley Geochronology Center Special Publication No. 5.
Lund, K. (2004), Geology of the Payette National Forest and vicinity, west-central Idaho, 89 pp., U.S. Geological Survey Professional Paper 1666.
Lund, K., and L. Snee (1988), Metamorphism, structural development, and age of the continent-island arc juncture in west-central Idaho, in *Metamorphism and Crustal Evolution of the Western United States*, *Rubey Colloquium Series*, vol. 7, edited by W. G. Ernst, pp. 296–331, Prentice-Hall, Upper Saddle River, N. J.
Lund, K., M. A. Kuntz, C. A. Manduca, C. H. Gammons, K. V. Evans, R. G. Tysdal, G. R. Winkler, and J. J. Connor (1997), Geologic map of the western Salmon River mountains, valley and Idaho counties, west-central Idaho, U.S. Geological Survey, scale: 1:100,000. [Available at http://pubs.er.usgs.gov/publication/i2599.]
Lund, K., J. Aleinikoff, E. Yacob, D. Unruh, and C. Fanning (2008), Coolwater culmination: Sensitive high-resolution ion microprobe (SHRIMP) U-Pb and isotopic evidence for continental delamination in the Syringa Embayment, Salmon River suture, Idaho, *Tectonics*, *27*, TC2009, doi:10.1029/2006TC002071.
Ma, C. (2015), Structure, depositional age, and magmatism in the Sawtooth metamorphic complex, Idaho: Implications for Cordilleran tectonics in the northern U.S.A., PhD dissertation, 255 pp., Univ. of Florida, Gainesville, Fla. [Available at http://ufdc.ufl.edu//IR00007343/00001.]
Ma, C., P. Bergeron, D. Foster, B. Dutrow, P. Mueller, and C. Allen (2016), Detrital-zircon geochronology of the Sawtooth metamorphic complex, Idaho: Evidence for metamorphosed lower Paleozoic shelf strata within the Idaho batholith, *Geosphere*, *12*, 1136–1153, doi:10.1130/GES01201.1.
Manduca, C. A., M. A. Kuntz, and L. T. Silver (1993), Emplacement and deformation history of the western margin of the Idaho batholith near McCall, Idaho: Influence of a major terrane boundary, *Geol. Soc. Am. Bull.*, *105*, 749–765.
Mattinson, J. M. (2010), Analysis of the relative decay constants of ^{235}U and ^{238}U by multi-step CA-TIMS measurements of closed-system natural zircon samples, *Chem. Geol.*, *275*, 186–198.
McClelland, W. C., and J. S. Oldow (2004), *Displacement Transfer Between Thick- and Thin-Skinned Décollement Systems in the Central North American Cordillera*, *Geol. Soc., London, Spec. Publ*, vol. 227(1), pp. 177–195.
McClelland, W. C., and J. S. Oldow (2007), Late Cretaceous truncation of the western Idaho shear zone in the central North American Cordillera, *Geology*, *35*(8), 723–726.
McClelland, W., B. Tikoff, and C. Manduca (2000), Two-phase evolution of accretionary margins: Examples from the North American Cordillera, *Tectonophysics*, *326*, 37–55.
Metz, K. (2010), Metamorphic Rocks in the Sawtooth Mountains, Idaho, U.S.A.: A window into the Precambrian basement of southwest Laurentia, MS thesis, 273 pp., Louisiana State Univ., Baton Rouge, La. [Available at http://etd.lsu.edu/docs/available/etd-07012010-102256/.]
Montz, W. J., M. Kedenburg, B. Tikoff, S. Giorgis, J. Vervoort, R. Gaschnig, and A. Byerly (2013), The Deadwood deformation zone, central Idaho: Constraints on timing and fabric development, Geological Society of America Abstracts with Programs, vol. 45, 813 pp.

19449194, 2017, 3, Downloaded from https://agupubs.onlinelibrary.wiley.com/doi/10.1002/2016TC004264 by Auburn University Libraries, Wiley Online Library on [27/10/2022]. See the Terms and Conditions (https://onlinelibrary.wiley.com/terms-and-conditions) on Wiley Online Library for rules of use; OA articles are governed by the applicable Creative Commons License

Mueller, P. A., G. D. Kamenov, A. L. Heatherington, and J. Richards (2008), Crustal evolution in the southern Appalachian orogen: Evidence from Hf isotopes in detrital zircons, *J. Geol.*, *116*, 414–422.

Oldow, J. S., A. W. Bally, H. G. Avé Lallemant, and W. P. Leeman (1989), Phanerozoic evolution of the North American Cordillera: United States and Canada, in *The Geology of North America: An Overview*, *The Geology of North America*, edited by A. W. Bally and A. R. Palmer, pp. 139–232, Geol. Soc. Am., Boulder, Colo.

Oldow, J. S., A. W. Bally, and H. G. Avé Lallemant (1990), Transpression, orogenic float, and lithospheric balance, *Geology*, *18*, 991–994.

Paces, J. B., and J. D. Miller (1993), Precise U-Pb ages of Duluth Complex and related mafic intrusions, northeastern Minnesota: Geochronological insights to physical, petrogenetic, paleomagnetic, and tectonomagmatic processes associated with the 1.1 Ga midcontinent rift system, *J. Geophys. Res.*, *98*, 13,997–14,013, doi:10.1029/93JB01159.

Passchier, C. (2001), Flanking structures, *J. Struct. Geol.*, *23*, 951–962.

Paterson, S. R., R. H. Vernon, and O. T. Tobisch (1989), A review of criteria for the identification of magmatic and tectonic foliations in granitoids, *J. Struct. Geol.*, *11*, 349–363.

Reid, R. R. (1963), Reconnaissance geology of the Sawtooth Range, Idaho Bureau of Mines and Geology Pamphlet 129, 39 pp. [Available at http://www.idahogeology.org/PDF/Pamphlets_(P)/P-129.pdf.]

Saint Blanquat, M., B. Tikoff, C. Teyssier, and J. L. Vigneresse (1998), *Transpressional Kinematics and Magmatic Arcs*, *Geol. Soc. London, Spec. Publ.*, vol. 135, pp. 327–340.

Saleeby, J. B., and C. Busby-Spera (1992), Early Mesozoic tectonic evolution of the western U.S. Cordillera, in *The Cordilleran Orogen: Conterminous U.S*, vol. G3, edited by B. C. Burchfiel, P. W. Lipman, and M. L. Zoback, pp. 107–168, Geol. Soc. Am., Boulder, Colo.

Sanderson, D. J., and W. Marchini (1984), Transpression, *J. Struct. Geol.*, *6*, 449–458.

Schmidt, K. L., R. S. Lewis, J. D. Vervoort, T. A. Stetson-Lee, Z. D. Michels, and B. Tikoff (2016), Tectonic evolution of the Syringa embayment in the central North American Cordilleran accretionary boundary, *Lithosphere*, doi:10.1130/l545.1.

Selverstone, J., B. P. Wernicke, and E. A. Aliberti (1992), Intracontinental subduction and hinged unroofing along the Salmon River suture zone, west central Idaho, *Tectonics*, *11*, 124–144, doi:10.1029/91TC02418.

Teyssier, C., B. Tikoff, and M. Markley (1995), Oblique plate motion and continental tectonics, *Geology*, *23*, 447–450.

Tikoff, B., and D. Greene (1997), Stretching lineations in transpressional shear zones: An example from the Sierra Nevada Batholith, California, *J. Struct. Geol.*, *19*, 29–39.

Tikoff, B., and C. Teyssier (1994), Strain modeling of displacement-field partitioning in transpressional orogens, *J. Struct. Geol.*, *16*, 1575–1588.

Tikoff, B., P. Kelso, C. Manduca, M. J. Markley, and J. Gillaspy (2001), *Lithospheric and Crustal Reactivation of an Ancient Plate Boundary: The Assembly and Disassembly of the Salmon River Suture Zone, Idaho, U.S.A*, *Geol. Soc. London, Spec. Publ.*, vol. 186, pp. 213–231.

Umhoefer, P. J. (2000), Where are the missing faults in translated terranes?, *Tectonophysics*, *326*, 23–35.

Vallier, T. L. (1995), Petrology of pre-Tertiary igneous rocks in the Blue Mountains region of Oregon, Idaho, and Washington: Implications for the geologic evolution of a complex island arc, in *Geology of the Blue Mountains Region of Oregon, Idaho, and Washington: Petrology and Tectonic Evolution of Pre-Tertiary Rocks of the Blue Mountains Region*, *U.S. Geological Survey Professional Paper*, vol. 1438, edited by T. L. Vallier and H. C. Brooks, pp. 125–209, Government Publishing Office, Washington, D. C.

Vigneresse, J., and B. Tikoff (1999), Strain partitioning during partial melting and crystallizing felsic magmas, *Tectonophysics*, *312*, 117–132.

Wright, J. E., and S. J. Wyld (2007), *Alternative Tectonic Model for Late Jurassic Through Early Cretaceous Evolution of the Great Valley Group, California*, *Geol. Soc. Am. Spec. Papers*, vol. 419, pp. 81–95.

Wyld, S. J., and J. E. Wright (2001), New evidence for Cretaceous strike-slip faulting in the United States Cordillera and implications for terrane-displacement, deformation patterns, and plutonism, *Am. J. Sci.*, *301*, 150–181.

Wyld, S. J., P. J. Umhoefer, and J. E. Wright (2006), Reconstructing northern Cordilleran terranes along known Cretaceous and Cenozoic strike-slip faults: Implications for the Baja British Columbia hypothesis and other models, in *Paleogeography of the North American Cordillera: Evidence for and Against Large-Scale Displacements*, *Geol. Assoc. Can. Spec. Pap.*, vol. 46, edited by J. W. Haggart, R. J. Enkin, and J. W. H. Monger, pp. 277–298, Geological Association of Canada, St. John's.

19449194, 2017, 3, Downloaded from https://agupubs.onlinelibrary.wiley.com/doi/10.1002/2016TC004264 by Auburn University Libraries, Wiley Online Library on [27/10/2022]. See the Terms and Conditions (https://onlinelibrary.wiley.com/terms-and-conditions) on Wiley Online Library for rules of use; OA articles are governed by the applicable Creative Commons License